

Characterization of connexin36 gap junctions in the human outer retina

Orsolya Kántor¹ · Zsigmond Benkő^{2,3} · Anna Énzöly^{4,5} · Csaba Dávid⁵ · Angela Naumann^{6,7} · Roland Nitschke^{6,7} · Arnold Szabó⁵ · Emese Pálfi¹ · József Orbán^{8,9} · Miklós Nyitrai^{8,9} · János Németh⁴ · Ágoston Szél⁵ · Ákos Lukáts⁵ · Béla Völgyi^{9,10,11,12}

Received: 20 December 2014 / Accepted: 6 July 2015 / Published online: 15 July 2015
© Springer-Verlag Berlin Heidelberg 2015

Abstract Retinal connexins (Cx) form gap junctions (GJ) in key circuits that transmit average or synchronize signals. Expression of Cx36, -45, -50 and -57 have been described in many species but there is still a disconcerting paucity of information regarding the Cx makeup of human retinal GJs. We used well-preserved human postmortem samples to characterize Cx36 GJ constituent circuits of the outer plexiform layer (OPL). Based on their location, morphometric characteristics and co-localizations with outer retinal neuronal markers, we distinguished four populations of Cx36 plaques in the human OPL. Three of these were comprised of loosely scattered Cx36 plaques; the distal-most population 1 formed cone-to-rod GJs, population 2 in the mid-OPL formed cone-to-cone GJs, whereas the proximalmost population 4 likely connected bipolar cell dendrites. The fourth population (population 3) of Cx36 plaques conglomerated beneath cone pedicles and connected dendritic tips of bipolar cells that shared a common

presynaptic cone. Overall, we show that the human outer retina displays a diverse cohort of Cx36 GJ that follows the general mammalian scheme and display a great functional diversity.

Keywords Gap junction · Electrical synapse · Photoreceptor · Cone · Rod · Bipolar cell

Introduction

Gap junctions (GJ) are conduits between cells that allow the free intercellular diffusion of ions and small molecules up to 1 kDa (Furshpan and Potter 1957; Watanabe 1958). They are formed at sites of close cell membrane appositions with a very narrow (1–2 nm) gap between contacting membrane surfaces. Connexons (hemichannels) are hexameres of connexin (Cx) protein subunits, each possessing

✉ Béla Völgyi
volgyi01@gamma.ttk.pte.hu; volgyb01@med.nyu.edu

¹ Department of Anatomy, Histology and Embryology, Semmelweis University, Budapest 1094, Hungary

² Department of Theory, Wigner Research Center for Physics of the Hungarian Academy of Sciences, Budapest 1121, Hungary

³ Semmelweis University School of Ph.D. Studies, Budapest 1085, Hungary

⁴ Department of Ophthalmology, Semmelweis University, Budapest 1085, Hungary

⁵ Department of Human Morphology and Developmental Biology, Semmelweis University, Budapest 1094, Hungary

⁶ Life Imaging Center, Center for Biological Systems Analysis, Albert-Ludwigs University, 79104 Freiburg, Germany

⁷ BIOS Centre for Biological Signalling Studies, Albert-Ludwigs-University Freiburg, 79104 Freiburg, Germany

⁸ Department of Biophysics, University of Pécs, Pécs 7624, Hungary

⁹ János Szentágothai Research Center, University of Pécs, Ifjúság str. 6, 7624 Pécs, Hungary

¹⁰ MTA-PTE NAP B Retinal Electrical Synapses Research Group, Pécs 7624, Hungary

¹¹ Department of Experimental Zoology and Neurobiology, University of Pécs, Pécs 7624, Hungary

¹² Department of Ophthalmology, New York University Langone Medical Center, New York, NY 10016, USA

four transmembrane domains, one intra- and two extracellular loops and intracellular C- and N-terminal endings. Two connexons of neighboring cells coalesce to form functional channels, whose conductance is largely determined by the makeup of the connexin constituents and the intracellular molecular milieu (Cruciani and Mikalsen 2006; Söhl and Willecke 2003). Over 20 Cx genes have been sequenced in various mammals (Söhl and Willecke 2003) and the gene product protein sequences are named after their molecular weights between 21 and 70 kDa (e.g., Cx43, Cx26, etc.). Retinal GJs have been shown to play a number of roles in signal processing, including transmission, averaging and synchronization of signals (Bloomfield and Völgyi 2009). In the mammalian retina, Cx36 and Cx45 have been found in both plexiform layers (Güldenagel et al. 2000; Petrasch-Parwez et al. 2004), whereas Cx50 and Cx57 (Massey et al. 2003; Hombach et al. 2004) are restricted to the outer plexiform layer (OPL) and Cx30.2 is found only in the inner plexiform layer (IPL) (Müller et al. 2010). Cx36 and Cx45 have been shown to process rod-mediated signals between AII amacrine and ON cone bipolar cells (BC) and between rod and cone photoreceptors (Feigenspan et al. 2001, 2004; Güldenagel et al. 2001; Mills et al. 2001; Deans et al. 2002; Lee et al. 2003; Völgyi et al. 2004; Han and Massey 2005; Maxeiner et al. 2005; Lin et al. 2005; O'Brien et al. 2012), and also serve to correlate ganglion cell signals (Hidaka et al. 2004; Schubert et al. 2005a, b; Völgyi et al. 2005, 2009, 2013a, b; Pan et al. 2010).

It has been shown that the human retina, similar to those of other mammalian species, expresses Cx36 both in the IPL and OPL (Söhl et al. 2010), and the distribution of immunostained plaques resembled patterns found previously in the mouse, rabbit, rat and the monkey (Feigenspan et al. 2001; Mills et al. 2001; Deans et al. 2002; Kihara et al. 2006, 2010; O'Brien et al. 2012; Kovács-Öller et al. 2014). However, it has been difficult to obtain details on the GJ forming neurons of the human retina due to the postmortem decomposition of available tissue. Therefore, it is unclear if the human retina shares the electrical circuit design described in other mammalian species. Such comparison is particularly important when mammalian animal models are in use to examine clinically relevant retinal conditions or to study human visual information processing. To this end, we obtained human retinal samples with minimal postmortem period (2–3 h) and performed multiple label immunohistochemistry to characterize Cx36-expressing neurons. Results of this immunohistochemical analysis on the outer retina are summarized in this manuscript, whereas findings regarding the inner retina will be detailed in a following study. We distinguished four populations of Cx36 plaques in the human outer retina. Plaques of population 1 were scattered throughout the distal part of

the OPL and often showed co-localizations with cone axons whereas population 2 consisted of Cx36 plaques that colocalized with cone pedicles in the mid-OPL area. While plaques of population 2 regularly connected neighboring cone terminals, some Cx36 plaques of population 1 connected cone photoreceptors to neighboring rods. In contrast to population 1 and 2, members of the third population (population 3) were rather arranged in laterally extended conglomerates just beneath cone terminals. These latter plaques colocalized with dendritic tips of various types of cone BCs that shared the same presynaptic cone photoreceptor. A fourth Cx36 plaque population (population 4) was scattered in the proximal-most OPL area and was associated with preterminal BC dendrites. Overall, the distribution of Cx36 plaques in the human retina displayed similarities to those of other mammals and showed a wealth of Cx36 GJs in the first synaptic layer of the human retina.

Materials and methods

Human patients

Human donor tissue from patients with no reported history of eye disease, collected for corneal transplantation, was used in this study, in accordance with the tenets of Declaration of Helsinki. After the removal of the cornea and the lens, the posterior eyecup was placed into fixative (4 % paraformaldehyde diluted in 0.1 M phosphate buffer (PB) (for 2 h at +4 °C) within 2–3 h after exitus. All personal identifiers were removed and samples were coded before histological processing. Retinas from four patients were investigated in this study (2 males, 2 females, age 27–59 years, postmortem time 2–3 h). The experimental protocol was approved by the local ethics committee of the Semmelweis University (TUKEB 58/2006).

Histological preparation

After fixation, specimens were rinsed several times in PB, the vitreous body was carefully removed and eyecups were radially cut into six pieces. For whole-mounts, the retina was carefully isolated from the mediotemporal parafoveal and peripheral area of the eye ball and the pigment epithelium was gently removed. The tissue was cut into small pieces, soaked overnight in 30 % sucrose in 0.1 M PB at +4 °C and stored in cryoprotectant solution at –20 °C for further use. For sections, inferonasal retinal pieces were placed into 30 % sucrose in PB at +4 °C then embedded in Tissue Tek (Sakura Finetek Europe B. V., Alphen aan den Rijn, The Netherlands). Blocks were stored at –80 °C until sectioning. 10–20 µm sections were cut in

the radial plane with a cryostat (Leica CM 1950, Leica Microsysteme, Wetzlar, Germany), mounted on gelatine-coated slides and stored at $-20\text{ }^{\circ}\text{C}$ until processing.

Immunohistochemistry

Fluorescent immunohistochemical reactions were carried out in sections and in whole-mounts according to standard protocols (Kántor et al. 2006). To enhance penetration in the whole-mounts, tissue was digested with 1 % pepsin solution for 15 min at $37\text{ }^{\circ}\text{C}$ and increased rinsing and incubation times were applied. Sections or tissue samples were washed several times with PBS (25 mM with 0.2 % Triton X; PBS-TX). Nonspecific staining was blocked in 10 % donkey serum diluted in PBS-TX. Afterwards, specimens were incubated in the primary antibodies at $+4\text{ }^{\circ}\text{C}$ (60 h for sections and 72 h for whole-mounts). Primary antibodies used in the present work are listed in Table 1. After extensive rinsing, specimens were incubated with the appropriate mixture of the following secondary antibodies: donkey anti-mouse immunoglobulin G (IgG) conjugated with Alexa 488, donkey anti-rabbit IgG conjugated with Alexa 555 or DyLight 649, donkey anti-guinea pig IgG conjugated with Alexa 555 (all Alexa conjugated antibodies were purchased from Life Technologies, Budapest, Hungary and all DyLight conjugated antibodies from Jackson ImmunoResearch Europe Ltd., Suffolk, UK) diluted in PBS-TX and 3 % normal donkey serum. Sections were incubated for 3 h at room temperature, whereas whole-mounts were incubated overnight, at $+4\text{ }^{\circ}\text{C}$. After several rinsing steps, whole-mounts were mounted on gelatine-coated slides and all specimens were coverslipped using AquaPolymount (Polysciences Europe GmbH, Eppelheim, Germany) as mounting medium. Slides were kept at $+4\text{ }^{\circ}\text{C}$ prior to imaging.

In cases when the utilized primary antibodies were raised in the same species (e.g., anti-connexin36 and anti-protein kinase C alpha (PKC α) were both raised in mouse) fluorescent tyramide signal amplification (TSA) was carried out according to Hunyady et al. (1996). Briefly, first we carefully titrated the dilution of the first primary antibody (anti-PKC α) to determine the dilution where conventional immunostaining resulted in no detectable signal. We then used the first primary antibody at this dilution (50 times more diluted than used for conventional immunohistochemistry) with biotin-TSA. After washing, sections were incubated with biotinylated goat anti-mouse IgG for 1 h at room temperature (1:500; Vector Laboratories, Burlingame, CA, USA). After extensive rinses, TSA was carried out using a TSA Kit (Life Technologies Hungary Ltd, Budapest, Hungary) according to the manufacturer's manual and using Cy5 conjugated streptavidin as

fluorophore (1:300, 3-h incubation; Jackson ImmunoResearch Laboratories Inc., West Grove, PA, USA). Subsequently, conventional fluorescent immunohistochemistry (anti-Cx36) was applied on the sections.

To visualize cones on whole-mounts, we performed lectin histochemistry using biotinylated peanut agglutinin (PNA; 1:10, Sigma-Aldrich Ltd., Budapest, Hungary) and Cy5 conjugated streptavidin (1:300; Jackson ImmunoResearch Europe Ltd., Suffolk, UK). In some sections, after the immunohistochemical reactions nuclei were stained using 4',6-diaminido-2-phenylindole (DAPI, 1:1000 for 10 min at room temperature; Sigma-Aldrich Co., Budapest, Hungary).

Imaging

Images were captured utilizing a confocal microscope (Zeiss LSM 510 Meta and Zeiss 710 with upright microscope Axio Imager Z1, Carl Zeiss Microscopy, Jena, Germany), 63 \times Plan-Apochromat oil-immersion lens (NA: 1.4) and the ZEN 2010 software (Carl Zeiss Microscopy, Jena, Germany). Alternatively, a Bio-Rad Radiance 2100 Rainbow confocal laser scanning system (Bio-Rad Laboratories, Hemel Hempstead, UK) and a 60 \times (NA: 1.4) oil-immersion objective attached to a Nikon Eclipse E800 microscope was utilized to obtain images. Voxel sizes in Z-stacks were $84 \times 84 \times 250\text{ nm}$. Final images were constructed using Adobe Photoshop 7.0 (San Diego, CA, USA). Only minor adjustments of brightness and contrast were applied and did not alter the original appearance of the images.

Image deconvolution was carried out utilizing the Huygens Software (Scientific Volume Imaging B. V., Hilversum, The Netherlands) and using classical deconvolution methods.

To detect the colocalization of Cx36 with either PKC α , Rec or CaB labeled structures raw data were analyzed using the ZEN 2012 software (Carl Zeiss Microscopy, Jena, Germany). Fifty Cx36 plaques per stack were randomly chosen in the OPL for analysis. Colocalization was suggestive if the maximal staining intensity of the Cx36 dot appeared in the same focal plane (Z dimension) as the maximal intensity of the secondary marker (PKC α , Rec or CaB) and no black pixels were detected between the two labeled structures. Orthogonal views of the stacks were generated and putative colocalizing sites were verified by measurements of the staining intensities. Histograms of staining intensities were generated along the Z axis. Colocalization of stainings was declared if the peaks of the histograms were found to be less than 9 pixels apart (750 nm, corresponding to the axial resolution limit of the confocal microscope). Note that orthogonal views were rescaled by ZEN to avoid image distortion; thus the

Table 1 Antibodies used in the present study

Antibody	Source	Host	Concentration
Anti-connexin 35/36 (Cx36) clone 8F6.2	Millipore, Temecula, CA, USA	Mouse monoclonal	1:1000
Anti-short wavelength sensitive opsin (SO)	Millipore, Temecula, CA, USA	Rabbit polyclonal	1:1000
Anti-middle/long wavelength sensitive opsin (M/LO)	Millipore, Temecula, CA, USA	Rabbit polyclonal	1:1000
Anti-recoverin (Rec)	Generous gift of Karl-Wilhelm Koch	Rabbit polyclonal	1:2500
Anti-calbindin D-28k (CaB)	Swant, Bellinzona, Switzerland	Rabbit polyclonal	1:5000 (for sections) 1:1000 (for flat mounts)
Anti-calbindin D-28k (CaB)	Synaptic Systems, Göttingen, Germany	Guinea pig polyclonal	1:2000
Anti-protein kinase C alpha subunit (PKC α)	Santa Cruz Biotechnology Inc., Santa Cruz, CA, USA	Mouse monoclonal	1:1000 (for conventional immunohistochemistry) 1:50,000 (for BTA)
Anti-rod transducin (rTR)	Abcam, Cambridge, UK	Rabbit polyclonal	1:300
Anti-AMPA type glutamate receptor subunit-4 (GluA4N)	Frontier Institute Co., Ltd., Ishikari, Japan	Guinea pig polyclonal	1:500
Anti-metabotropic glutamate receptor 6 (mGluR6)	Generous gift of Noga Vardi	Rabbit polyclonal	1:3000

original Z voxel component (250 nm) was reduced to 84 nm to match the dimensions of the X – Y components.

Statistical analyses

Datasets were obtained from Z -stacks of radial sections ($n = 20$) where either M/L- or S-cones were specifically labeled. Numbers of labeled cones were manually counted and cone frequency numbers were calculated based on the width (determined by the field of view) and depth (determined by the thickness of the radial section; $\sim 10 \mu\text{m}$) dimensions for each stack. Cx36 plaques that colocalized with M/L- or S-cone pedicles or M/L-cone pedicle contacts were manually counted in stacks, averages and standard deviations were determined in Origin7 (Microcal Origin, Northampton, USA).

To perform analyses on the distribution of Cx36-immunolabeled plaques we obtained top views of $196 \mu\text{m} \times 196 \mu\text{m}$ frames of the OPL in whole-mount specimens. The image processing for morphometric analysis and the analysis itself were performed using Fiji (Schindelin et al. 2012). The Cx36-immunoreactive particles and the pedicles of photoreceptors were separated using a gray level watershed algorithm (Sage 2008) after application of Gaussian blurring 1.5 and 5.0, respectively. The area occupied by Cx36-immunoreactive particles belonging to a single photoreceptor pedicle were measured

with the convex hull plugin of Fiji, and the parameters of the particles and clusters (area, coordinates, gray intensity level, form description) were exported into an excel spreadsheet. We then estimated the probability density function ($P(x)$) of the pedicle area, the convex hull area and the number of Cx36 plaques with a weighted sum of log-normal components for each case:

$$P(x) = \sum_{k=1}^K \pi_k \cdot p_k(x),$$

where K is the number of components and π_k is the mixing coefficient of the k -th component. The coefficients are normalized, that is $\sum_{k=1}^K \pi_k = 1$. $p_k(x)$ -s are the log-normal components which are given by:

$$p_k(x) = \frac{1}{x\sigma_k\sqrt{2\pi}} \cdot e^{-\frac{(\ln(x)-\mu_k)^2}{2\sigma_k^2}},$$

where μ and σ are the location and the shape parameters of the distribution, respectively. We fitted the model through maximization of the likelihood given the model using an iterative procedure called the Expectation Maximization (EM) algorithm. The likelihood is the probability of the data set given the parameters:

$$L = P(\text{Data}|\pi, \mu, \sigma) = \prod_{n=1}^N P(x_n)$$

The data set is the co-occurrence of observed data points (x_n), so the probability of the data set is the product of the N individual data-point probabilities (here, we assumed that the data points are independent and identically distributed).

We initialized the parameters randomly and then waited 800 iteration steps, this procedure was repeated 20 times and the solution with maximal likelihood was accepted. We performed the above procedure for a different number of components (from 1 to 9). The optimal number of components (K^*) was chosen according to the Bayesian Information Criterion (BIC). BIC shows the optimality of a model by introducing a tradeoff between the likelihood and model complexity:

$$BIC(K) = -2 \cdot \ln(L) + (3K - 1) \cdot \ln(N)$$

The first term on the right-hand side is the negative logarithm of the likelihood, which is a monotonically decreasing function of K . In the second term is the number of free fitted parameters, namely the log-scale, the shape and the mixing coefficient for each component and minus one due to the normalization restriction for mixing coefficients. This latter term is a monotonically increasing function of K , acting as a penalty for the number of parameters, which is a simple estimate of model complexity. The optimal model has the smallest BIC value.

Two population t test and fitting of a linear regression line were performed in Origin7 (Microcal Origin, Northampton, USA). $p < 0.05$ was considered as significant.

Reconstruction of Cx36 plaques

For detailed description of the Cx36 plaques distribution within the OPL, four confocal stacks of sections stained for Cx36, M/LO and DAPI and imaged under identical conditions (oversaturated pixels were strictly avoided) were 3D reconstructed using Neurolucida (version 11; MicroBrightField Europe, Magdeburg, Germany). 794 Cx36 plaques were mapped in total. Plaque numbers and sizes were calculated using NeuroExplorer (version 11; MicroBrightField Europe, Magdeburg, Germany). Distance of individual plaques from the borders of OPL was also determined.

Results

Photomicrographs of this study depict central human retinal areas unless it is specified otherwise. As a result, staining patterns for each neuronal marker were identical in all retinal samples of this study.

Cx36 distribution in the human retina

To detect Cx36 GJ sites in the human retina, Cx36 immunohistochemistry was carried out utilizing a monoclonal antibody raised against the perch Cx35. This anti-serum has been widely used to recognize Cx36 GJs in the nervous tissue of various mammals including macaque (O'Brien et al. 2012; Rash et al. 2012; Kovács-Öller et al. 2014; Pereda et al. 2003). Similar to other species, the antibody recognized a number of Cx36 GJ plaques in both plexiform layers of the human retina (Fig. 1a–d). While a detailed description of Cx36 immunolabels in the IPL will be given in another manuscript, this work focuses on Cx36 labeling of the human outer retina. The majority of Cx36 plaques in the OPL were arranged into horizontally extended strip-like conglomerates (Fig. 1e, f) in the middle of the OPL (Table 2, bottom). In addition, three populations of solitary Cx36 plaques were found: one in the distal, one in the middle and one in the proximal OPL (Fig. 1e, f; Table 2, bottom). Thus, in the following sections, we will refer to the distal plaques as population 1, to mid-OPL plaques as population 2, to the conglomerate forming Cx36 plaques as population 3 and to the proximal plaques as population 4. Four stacks from paracentral retinal specimen were selected to perform plaque counts, plaque size measurements (plaque diameter) and to determine the location of Cx36 plaques in the OPL (% depth of OPL). The number counts and relative contributions of Cx36 plaques to each population are shown in Table 2. The conglomerate forming population 3 plaques accounted for almost half of the Cx36 plaques in the OPL, whereas population 1, 2 and 4 contributed with ~ 10 , 20 and 20 %, respectively. All plaques, regardless the population fell in the 0.29–0.36 μm range with population 1 plaques amongst the smallest and population 3 plaques amongst the largest ones. Since the measurements of confocal microscopy are not adequate to determine absolute plaque sizes we did not perform statistical analysis for the significance of differences.

Detection of cone photoreceptors in the human retina

Photoreceptors in most examined mammalian species form GJs, and some of these connect either cones or rods into small focal arrays, whereas others signal between rods and cones and serve the secondary rod-signaling pathway (Bloomfield and Völgyi 2009; Völgyi et al. 2013a). To identify such contacts in the human retina, conventional cone markers were tested first. Cone photoreceptors have been successfully detected with antibodies that recognize the calcium binding protein calbindin (CaB) in other mammals (Massey and Mills 1996; Völgyi et al. 1997; Grünert et al. 1994) and in the human retina (Haverkamp

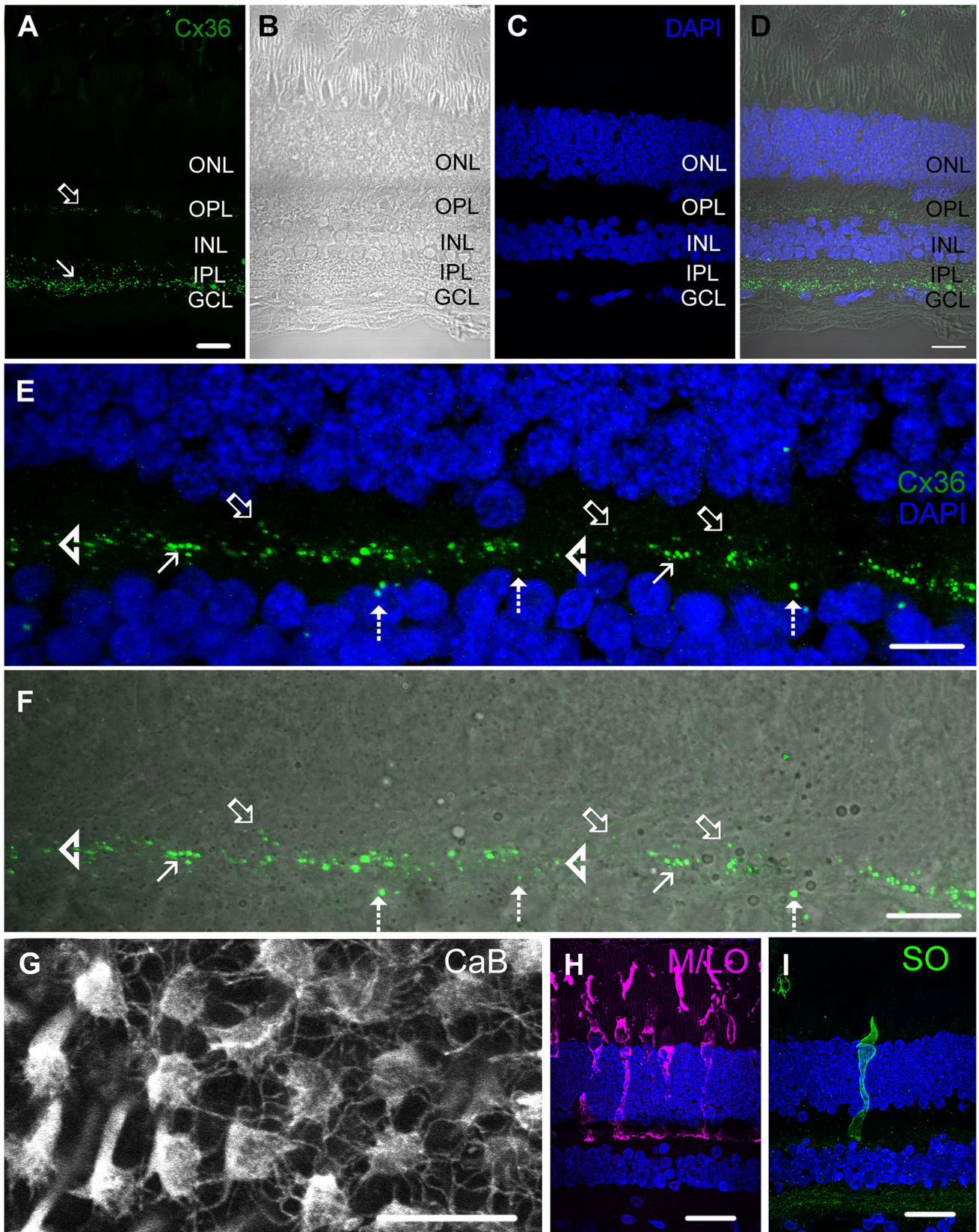


Fig. 1 Connexin36 immunoreactivity in the human retina. **a–f** Photomicrographs showing epifluorescent (**a**, **c**), DIC (**b**) and composite (**d**) images of a Cx36 (green) and DAPI (blue) labeled radial section of the human retina. Cx36 immunolabeled plaques are evident in both the OPL (open arrow) and the IPL (arrow). **e–f** Enlarged view of a radial section showing the distribution of Cx36 immunolabeled plaques in the OPL. Solitary Cx36 plaques are located in the proximal OPL (closer to the vitreous, dashed arrows) in the mid-OPL (arrowhead) and distal OPL (closer to the photoreceptor somata, open arrows), whereas characteristic strip-like (or disc-shaped) conglomerates of Cx36 plaques (arrows) are found in the mid-OPL. This juxtaposition of Cx36 conglomerates as well as the proximal subset of solitary plaques to the INL is even more obvious when a DIC view is overlaid (**f**). **g** Flat-mount view of the human retina showing the CaB⁺ cone pedicles. Telodendria reach out radially towards neighbouring photoreceptors, giving a spider-like appearance to pedicles. **h**, **i** Epifluorescent views of a radial section of the human retina. M/L-cones (purple) are stained for the M/LO (DAPI labeled nuclei are blue), whereas S-cones are distinguished by their SO (green) staining. ONL outer nuclear layer, OPL outer plexiform layer, INL inner nuclear layer, IPL inner plexiform layer, GCL ganglion cells layer. **a–f** Maximal intensity projections (MIP) of nine optical sections (9 × 250 nm), **g–i** MIP of three optical sections (3 × 250 nm). Scale bar 20 μm

et al. 2003). CaB was expressed by a cohort of cone photoreceptors in our sample both in transversal sections and whole-mounts (Figs. 1g, 8a). Besides CaB, which labeled cones non-selectively, medium/long wavelength-sensitive (M/L) and short wavelength-sensitive (S) cones were distinguished by using antibodies against green/red opsin (M/LO; M and L cones can not be distinguished by immunohistochemistry due to the high amino acid sequence homology of red and green opsins; Nathans et al. 1986) and blue opsin (SO), respectively (Fig. 1h, i). We found that S-cones of the human retina were somewhat smaller and had unusual-shaped pedicles (Fig. 1h, i) similar to primate S-cones (Ahnelt et al. 1987, 1990; Ahnelt and Kolb 1994; Bumsted and Hendrickson 1999; Hendrickson et al. 2007, 2009; Kolb et al. 1997; Xiao and Hendrickson 2000). In addition to the morphological characteristics, the SO antibody marked cones less frequently in all sections than the serum against M/LO (density of S-cones: $1127.8 \pm 353.9 \text{ mm}^2$, $n = 13$; density of M/L-cones $7548.7 \pm 2020.4 \text{ mm}^2$, $n = 17$). This, thus, indicated the specificity of our antibodies and their capability to discriminate between M/L and S-cones.

Cx36 colocalization with photoreceptor axon terminals

Next, we performed dual staining immunohistochemistry in sections to label Cx36 GJ sites associated with either M/L- or S-cones. We found that a number of Cx36 plaques were superimposed on M/L-cone pedicles (Fig. 2a–c; 2.87

Cx36 plaques/pedicle $\pm 1.5 \text{ SD}$, $n = 153$) or less frequently colocalized with S-cone pedicles (0.76 Cx36 plaques/pedicle $\pm 0.8 \text{ SD}$, $n = 42$; Fig. 2d–f; the counts were performed in sections thus they are likely underestimations). In the case of M/L-cones, colocalizing Cx36 plaques belonged to the solitary population 1 or 2 and were usually located on the side of pedicles or small telodendric protrusions. Moreover, population 2 Cx36 plaques were often found at sites where pedicles of two M/L-cones came into contact, indicating GJ sites between M/L-cones (Fig. 2b, c). In contrast, cone-to-cone contacts between S-cones were not detected due to the low S-cone density (Fig. 2d–f). Cone-to-cone contacts were further analyzed by dual staining whole-mount retinal samples by utilizing CaB and Cx36 antibodies. Besides the frequently observed conglomerates in sub-pedicle areas, we often found that population 2 solitary Cx36 plaques colocalized with cone telodendria (Fig. 3) or even located at cone-to-cone contact sites (Fig. 3c, d).

Interestingly, we found Cx36 plaques on M/L-cone pedicles that did not seem to contribute to the above cone-to-cone contacts. These Cx36 plaques were often located on the side or apical surface of cone telodendria or even more distal axonal areas but typically lacked contacts with other cones. These population 1 and 2 Cx36 plaques resembled to sites previously described as cone-to-rod GJs in the primate retina (O'Brien et al. 2012). In fact, we found that some rod spherules labeled with an antiserum against rod transducin (rTR) displayed a close vicinity to these Cx36 plaques (Fig. 4a, f). To examine if these are sites of rod-cone GJs, we counterlabeled the rTR/Cx36 retinal specimen with peanut agglutinin (PNA) that specifically binds to the galactose/*N*-acetylgalactosamine sequence of the cone carbohydrate matrix sheath. In fact, we encountered a number of triple colocalizations and/or close spherule/pedicle appositions with Cx36 plaques in key intermediate positions (Fig. 4a–e, g–i). In addition to the rTR/Cx36/PNA triple labeled whole-mounts, we also performed rTR/Cx36/CaB triple label experiments in radial retinal sections. We selected CaB labeled cone photoreceptors whose CaB staining could clearly be isolated from labeled processes of nearby CaB⁺ BCs and horizontal cells (HCs). We found that some of the selected sections displayed clear spherule/pedicle appositions with Cx36 colocalization (Fig. 4j–m). These experiments clearly indicated that Cx36 forms cone-to-rod GJs in the human OPL. The putative cone-to-rod GJs were comprised mostly by Cx36 plaques of population 1 and less frequently by population 2. We also encountered juxtapositions of spherule-plaque-spherule triplets that suggested the existence of Cx36 rod-to-rod GJs in the human retina (Fig. 4i).

Table 2 Statistical dataset of the four Cx36 plaque populations in the human OPL

Plaque count	Population 1	Population 2	Population 3	Population 4	Total plaque count
Stack3	36	56	134	86	312
Stack4	20	30	77	23	150
Stack5	13	47	94	25	179
Stack6	10	36	75	32	153
Total plaque count/%	79/9.9	169/21.3	380/47.8	166/20.9	794/100
Plaque size (μm)	Population 1	Population 2	Population 3	Population 4	
Stack3	0.305556	0.298214	0.363433	0.34186	
Stack4	0.3	0.313333	0.383117	0.308696	
Stack5	0.246154	0.3	0.36383	0.344	
Stack6	0.3	0.313889	0.365333	0.31875	
Average size/SD	0.29 \pm 0.07	0.3 \pm 0.05	0.36 \pm 0.08	0.33 \pm 0.07	
Plaque location in OPL depth (%)	Population 1	Population 2	Population 3	Population 4	
Stack3	48.7	70.6	76	80.7	
Stack4	46.95	58.9	63	72.7	
Stack5	54	64.3	67	80.3	
Stack6	47.7	58.3	66.1	71	
Average size/SD	49.1 \pm 12.41	64.2 \pm 10.27	69.1 \pm 10.4	77.7 \pm 9.63	

Note that values of each cell in middle and bottom tables represent average values for a cohort of plaques in one certain stack and population

Characterisation of subpedicle Cx36 conglomerates

Population 3 conglomerate forming Cx36 plaques were typically located right beneath cone pedicles. In this regard, M/L- and S-cones were similar, as sub-pedicle spaces of both cone populations were occupied by conglomerates (Fig. 2). S-cone pedicle-associated conglomerates were short and possessed less individual Cx36 plaques (4.35 ± 2.96 SD; $n = 42$), whereas those observed beneath M/L-cone pedicles extended further laterally and were composed of more plaques (11.75 ± 3.62 SD; $n = 153$). Note, that the above numbers of Cx36 plaques are underestimations, as measurements were performed in sections (some Cx36 plaque numbers corresponded to fractioned pedicles) and thus they only represent relative quantities. Overall, the location and structure of conglomerates were clearly associated with cone pedicles, even though they did not seem to colocalize.

To further characterize conglomerates we carried out Cx36 immunohistochemistry in whole-mount retinas and visualized conglomerates in randomly selected $196 \mu\text{m} \times 196 \mu\text{m}$ retinal areas ($n = 10$) from the mid-peripheral retina. In whole-mount specimen, conglomerates appeared disk- or crescent-shaped and were organized in a regular honeycomb-like fashion with rather regular spacing (Fig. 5a, b; mean distance = $46 \mu\text{m}$, $n = 107$). It was clear from the dual-

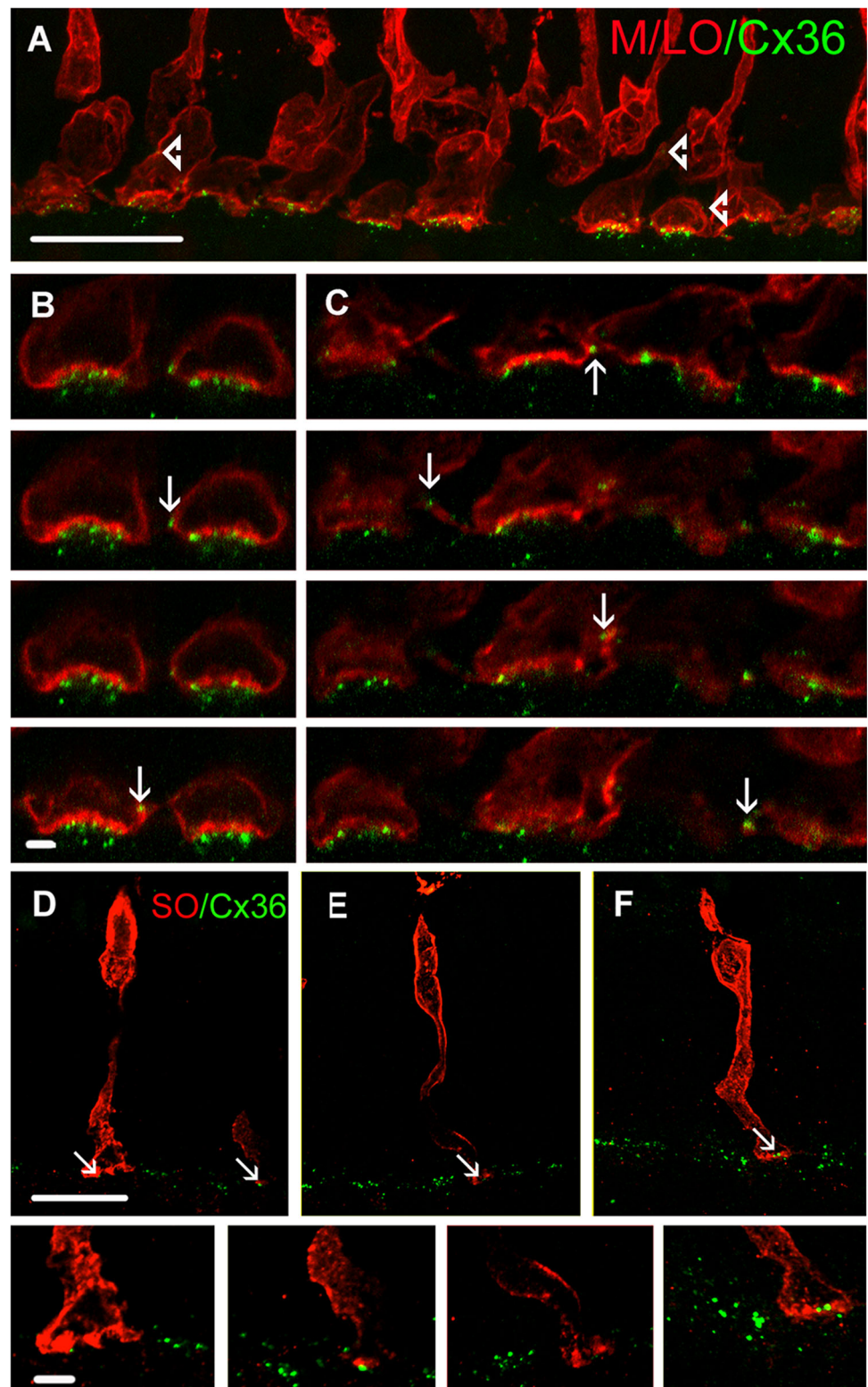
stained CaB/Cx36 specimen that each conglomerate was associated to a cone pedicle that located somewhat distally (scleral) from these structures (see also Fig. 2). To determine if there is a preferred conglomerate shape and/or intraconglomerate location of the individual Cx36 plaques, ten randomly selected pedicle/conglomerate pairs were stacked into a single image (Fig. 5c). This manipulation showed that Cx36 plaques in fact preferred central sub-pedicle spaces, whereas the peripheral location of Cx36 plaques was less likely (Fig. 5c). This feature was advantageous as it further helped to distinguish between population 2 and population 3 plaques.

To obtain more information on the variability of sub-pedicle Cx36 conglomerates we determined pedicle area sizes ($n = 379$), subpedicle Cx36 convex hull area sizes ($n = 379$) and the number of Cx36 plaques in subpedicle conglomerates. The probability density distributions of all three measures showed the marks of multimodality. Thus, we performed a mathematical model selection process to determine the optimal number of unicode components of the observed distributions (see “Materials and methods”). Since the Gaussian distribution can take both positive and negative values, but all three examined measures here (pedicle area, convex hull area and number of Cx36 plaques/pedicle) are restricted to positive values by definition, we chose lognormal distributions to describe the form of each component.

The selection process resulted in two components (minimum BIC value occurred at 2 log-normal components) for the optimal model of the pedicle area

distribution. This suggested the presence of two pedicle populations, including a less frequent population with smaller area sizes of $42.848 \mu\text{m}^2 (\pm 18.479 \mu\text{m}^2 \text{SD})$ and a

Fig. 2 The Cx36 plaque distribution in the OPL is strongly correlated with M/L- and S-cone pedicles. **a** M/L-cone pedicles (*red*) are associated with both solitary and aggregated Cx36 plaques (*green*). Cx36 conglomerates are located right below M/L-cone pedicles. *Arrowheads* indicate population 1 solitary plaques. **b, c** Sets of consecutive images of the same stack displaying the colocalization of population 2 (*arrows*) solitary Cx36 plaques with contacting telodendria of neighboring M/L-cones. **d–f** Images of S-cones, each displaying Cx36 plaques in the vicinity of their pedicles. However, S-cone pedicles are mostly associated with Cx36 plaques that contributed to short conglomerates but less frequently with solitary Cx36 plaques. *Arrows* point to locations enlarged in *insets* at the *bottom*. Images **a, d–f** are MIPs of two optical slices ($2 \times 250 \text{ nm}$), **b, c** and *insets* are single optical slices (250 nm). *Scale bar* $20 \mu\text{m}$ in **a, d, e, f** and $2 \mu\text{m}$ in **b, c** and **d–f** small images



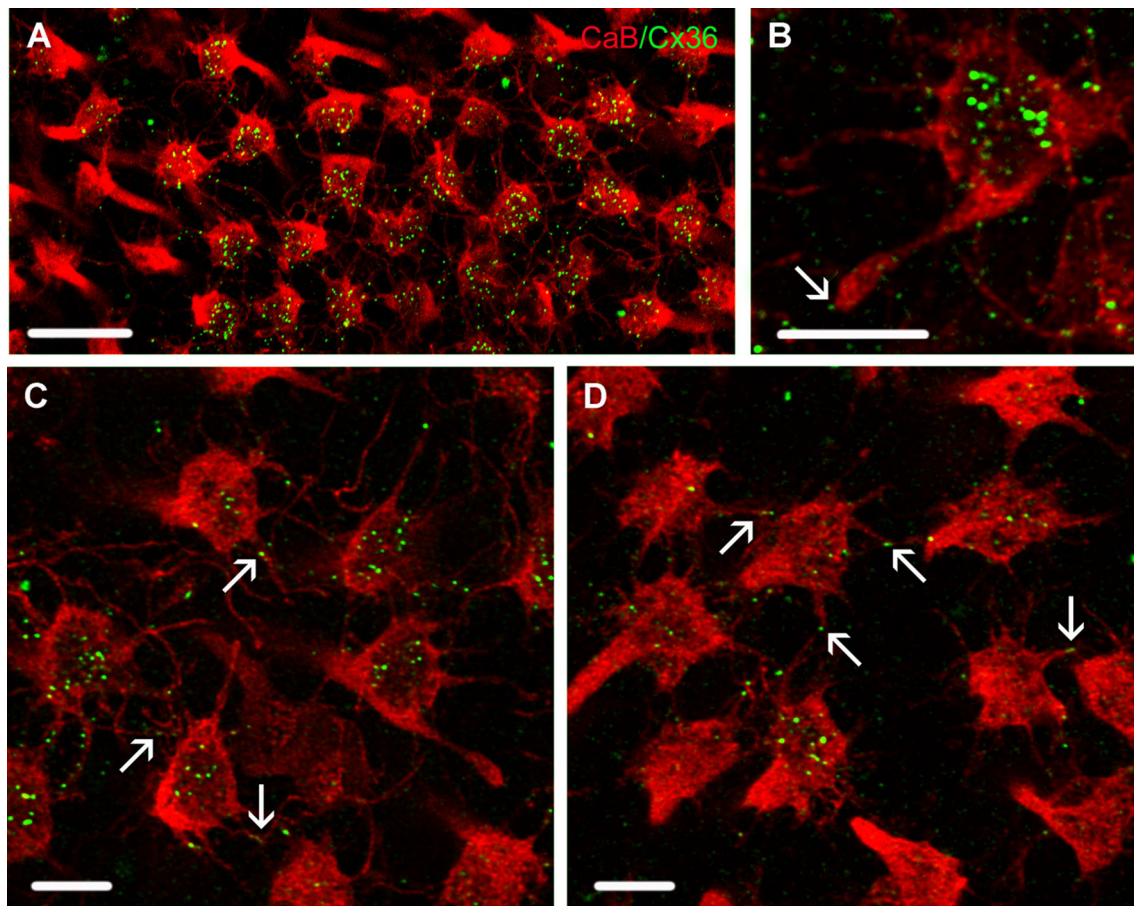


Fig. 3 Cx36 plaques are often localized in cone-to-cone contacts. **a** Flat mount overview of CaB⁺ cone pedicles (red) with Cx36 counterlabels (green). **b** Deconvolved high magnification image of the flat-mount retina reveals a Cx36 plaque (arrow) localized on the tip of a cone telodendrion without any apparent contact with

neighbouring cones. **c, d** Cone telodendria and population 2 Cx36 plaques are colocalized at cone-to-cone contacts (arrows). Flat-mount images are MIPs of three optical sections (3×250 nm). Scale bar **a, b** 10 μ m, **c, d** 5 μ m

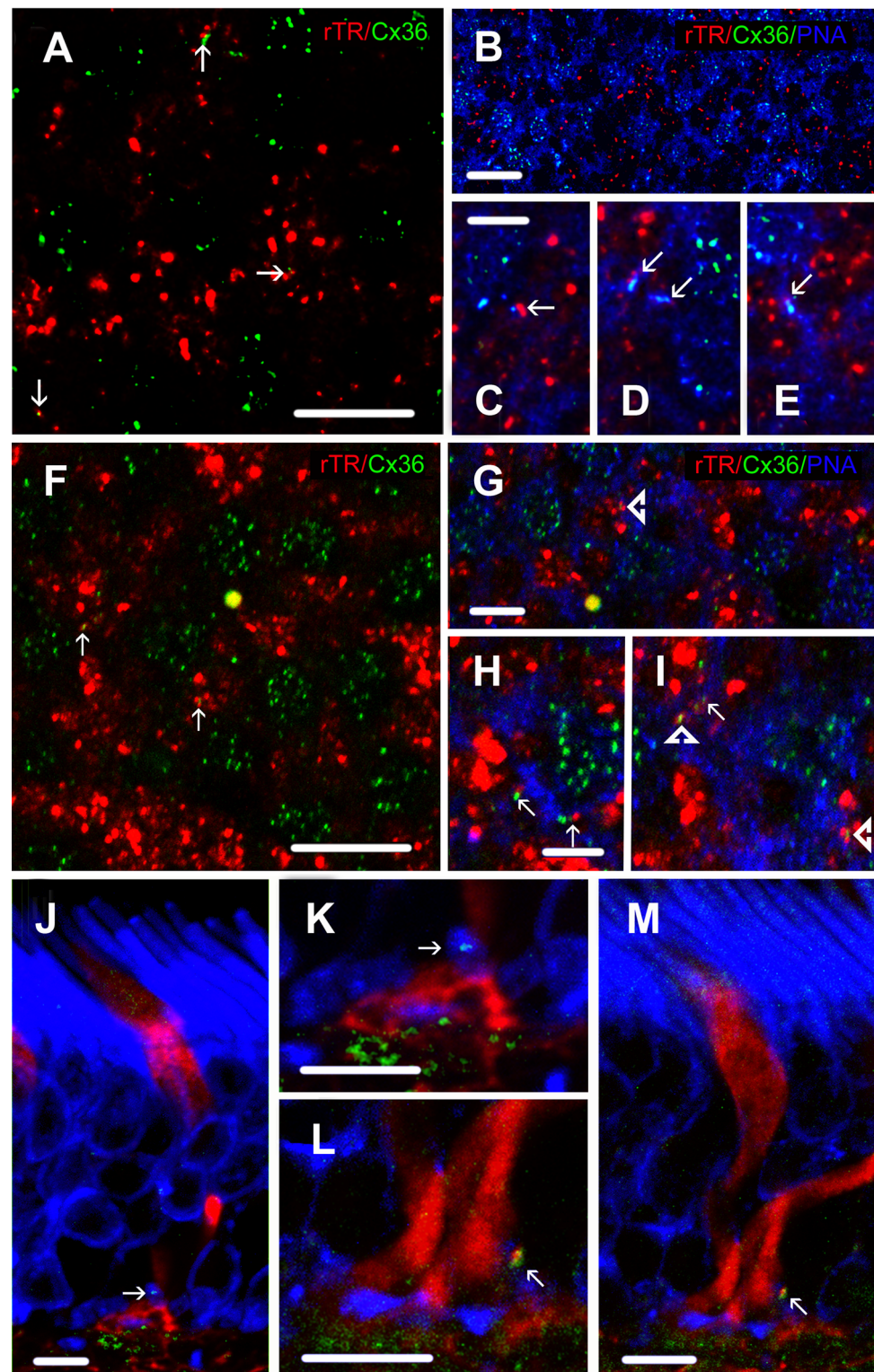
more numerous one with area sizes of $54.802 \mu\text{m}^2$ ($\pm 10.804 \mu\text{m}^2$ SD; Fig. 5d). Interestingly, a three components solution was the optimal choice when convex hull area size values were analyzed. The modes were at $0.166 \mu\text{m}^2$ ($\pm 1.226 \mu\text{m}^2$ SD), $19.62 \mu\text{m}^2$ ($\pm 15.667 \mu\text{m}^2$ - SD) and $31.678 \mu\text{m}^2$ ($\pm 5.811 \mu\text{m}^2$ SD). However, the first component was confined to small values that most likely corresponded to convex hull fragments, and the majority of the distribution was well described by two components (Fig. 5e). Thus, we concluded that two populations of subpedicle Cx36 conglomerates existed. Similarly, the optimal choice for the number of Cx36 plaques/pedicle dataset occurred for the three-components calculation with modes at 1.731 (± 2.065 SD), 9.048 (± 4.242 SD) and 17.455 (± 4.374 SD) (Fig. 5f). Again, the first component was too small and likely corresponded to conglomerate fragments. This latter analysis further supported the existence of two Cx36 conglomerate populations. Finally, we plotted the number of Cx36 plaques against conglomerate areas (see

“Materials and methods”). We found that the distribution of data points showed a quasi-linear relationship and could be fit with a linear regression line ($p < 0.0001$; Fig. 5f, inset). This reflected that the relative frequencies of Cx36 plaques in conglomerates are rather similar in the two putative subpopulations.

Cx36 conglomerate plaques are associated with postsynaptic glutamate receptors

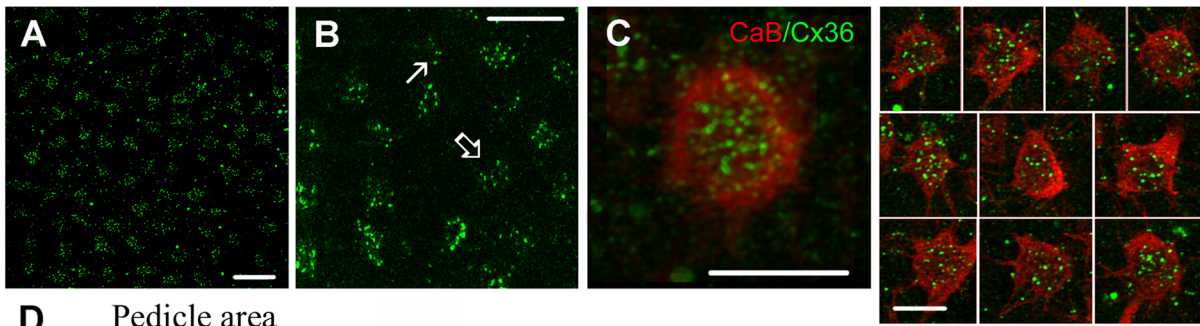
The subpedicle position of population 3, conglomerate forming Cx36 plaques suggested that they were expressed by bipolar cell dendritic tips. To examine this, we first performed a double label experiment to stain postsynaptic retinal mGluR6 receptors and Cx36 forming gap junctions. We found that the anti-mGluR6 serum stained relative large (~ 1 – $2 \mu\text{m}$ in diameter), mostly spherical structures that were scattered throughout the human OPL. These structures were very similar to those identified as rod

Fig. 4 Cx36 comprises cone-to-rod gap junctions. **a** Image displaying rod transducin-stained (rTR) rod spherules (red) and Cx36 immunolabeled population 1 plaques (green) in the distal portion of the OPL. Arrows point to rod spherules with nearby Cx36 plaques. **b–e** Triple labeling displays cone pedicles (PNA, blue), rod spherules (anti-rTR, red) and population 1 Cx36 (green) staining in the distal OPL (above the cone pedicles). Cone telodendria with Cx36 plaques contact rod spherules (arrows), indicating the existence of Cx36 GJs between rods and cones. **f** Image displaying rTR-stained rod spherules (red) and population 2 Cx36 immunolabeled plaques (green) in the middle portion of the OPL (at the level of the pedicles). Arrows point to rod spherules with nearby Cx36 plaques. **g–i** Triple labeling displays cone pedicles (PNA, blue), rod spherules (anti-rTR, red) and Cx36 (green) staining in the proximal OPL. Cone telodendria with Cx36 plaques contact rod spherules (arrows), indicating the existence of Cx36 GJs between rods and cones. Less frequently Cx36 plaques occurred in contact sites of two rod spherules (arrowheads). **j–m** Radial retinal sections display rTR labeled (blue) rods, CaB labeled cones (red) and Cx36 stained plaques (green). Some spherule/pedicle appositions display clear colocalizations (arrows) with population 1 and 2 Cx36 plaques that indicate the presence of Cx36 rod-cone GJs. Whole-mounts were collected from midperipheral, sections were obtained from the peripheral part of the retina. Scale bar 10 μ m for all images

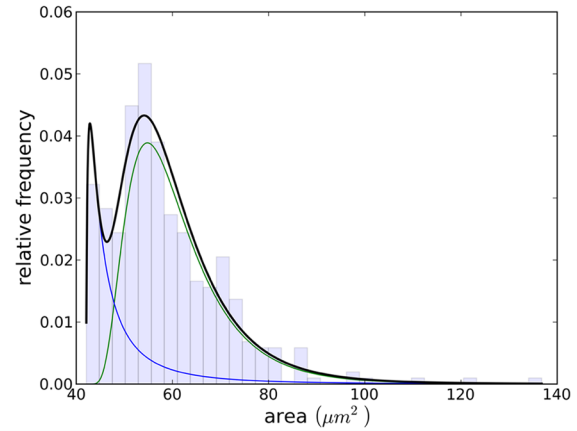
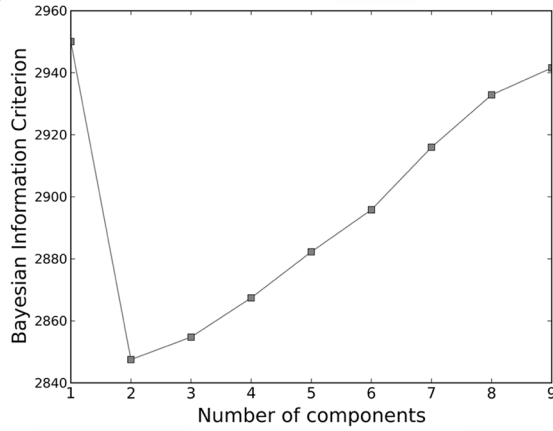


bipolar cell dendrite tips in the monkey retina (O'Brien et al. 2012; Fig. 6a). In addition, smaller mGluR6 plaques were also found that did not scatter but rather formed aggregates. Interestingly, plaques of mGluR6 aggregates and Cx36 conglomerates were entirely intermingled

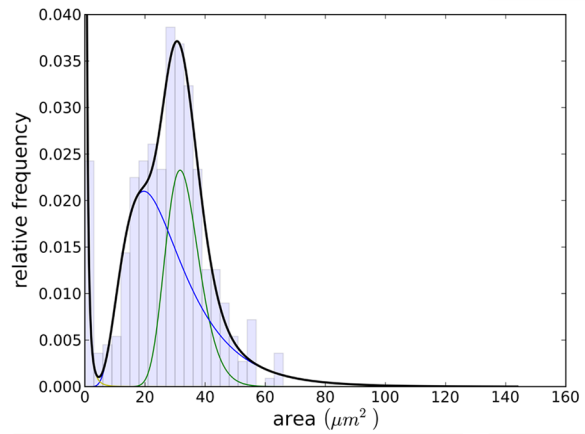
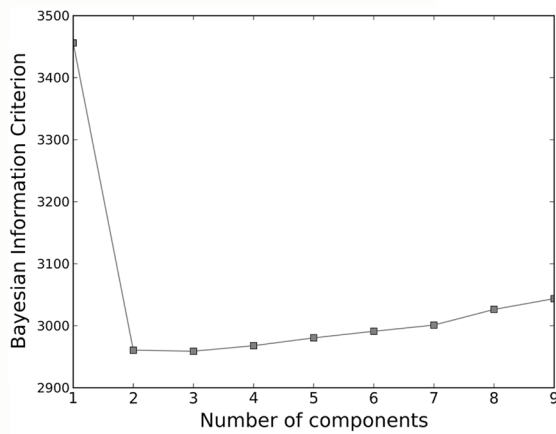
suggesting that both populations occupied subpedicle positions. This was confirmed by a triple labeling experiment, in which both mGluR6 and Cx36 conglomerate forming plaques were strictly associated with cone pedicles (Fig. 6b). Moreover, Cx36 plaques were often found in the



D Pedicle area



E Convex hull area



F Number of Cx36 puncta/pedicle

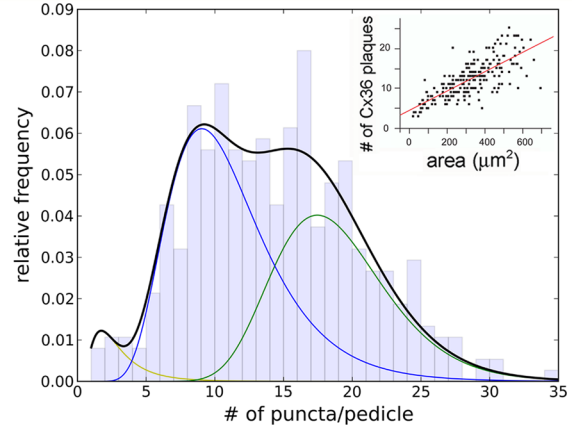
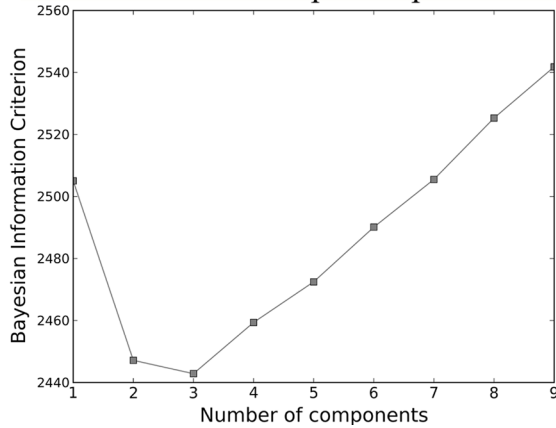


Fig. 5 Cx36 conglomerates are associated with cone pedicles. **a, b** A whole-mount view of the human OPL shows that Cx36 conglomerates are distributed in a highly regular fashion in the OPL. Some conglomerates display only a handful of Cx36 plaques (*arrow*), whereas others display a larger number of plaques (*open arrow*) (**b**). Images show MIPs of ten optical sections (10×250 nm). **c** Cx36 plaques (*green*) seem randomly distributed in conglomerates when CaB^+ (*red*) pedicles are viewed individually (small panels to the *right*). However, an overlay of ten pedicles shows that plaques prefer central subpedicle locations. **d** Values of Bayesian Information Criterion (BIC) for different numbers of constituent log-normal distributions were calculated for datasets of cone pedicle area sizes (*left*). The minimum of the BIC clearly occurred at 2 log-normal components, thus 2 was used as the number of functions in the following fitting process. The distribution of cone pedicle area sizes is visualized in the histogram on the *right*. The *solid black line* marks the estimated continuous probability density function, which is the weighted sum of the constituent log-normal distributions with maximums at $42.848 \mu\text{m}^2$ ($\pm 18.479 \mu\text{m}^2$ SD) and $54.802 \mu\text{m}^2$ ($\pm 10.804 \mu\text{m}^2$ SD) shown by blue and green, respectively. **e** Values of Bayesian Information Criterion (BIC) for different numbers of constituent log-normal distributions were calculated for datasets of convex hull area sizes (*left*). Similar low minimum BIC values occurred at 2 and 3 log-normal components. However, the smallest log-normal component was likely due to the presence of a convex hull fraction in the dataset. Thus, we rejected the smallest convex hull sizes and used 2 as the number of functions in the following fitting process. The distribution of convex hull area sizes of was visualized in the histogram on the *right*. The *solid black line* marks the estimated continuous probability density function, which is the weighted sum of the constituent log-normal distributions with maximums at $19.62 \mu\text{m}^2$ ($\pm 15.667 \mu\text{m}^2$ SD) and $31.678 \mu\text{m}^2$ ($\pm 5.811 \mu\text{m}^2$ SD) shown by blue and green, respectively. **f** Values of Bayesian Information Criterion (BIC) for different numbers of constituent log-normal distributions were calculated for datasets of Cx36 numbers/pedicle (*left*). The minimum BIC value occurred at 3 log-normal components. However, one component corresponded to convex hull fragments, thus in the following analysis we calculated with 2 log-normal distributions that occurred at the next smallest BIC value. The Cx36 plaques/pedicle distribution is visualized in the histogram on the *right*. The *solid black line* marks the estimated continuous probability density function, which is the weighted sum of the constituent log-normal distributions with maximums at 9.048 (± 4.242 SD) and 17.455 (± 4.374 SD) shown by blue and green, respectively. The *inset* on the *right* displays the largely linear relationship between the number of Cx36 plaques and the area of convex hulls, which indicates that the Cx36 density is similar in all conglomerates. *Scale bar* $20 \mu\text{m}$ in **a, b** and $15 \mu\text{m}$ in **c**

close vicinity of small mGluR6 plaques that suggested the proximity of neuronal structures (likely dendrites) that expressed them (Fig. 6c–j). It was also clear, that the larger mGluR6 stained spots do not overlap with cone pedicles further supporting the view that these latter mGluR6 spots corresponded to rod bipolar cell dendrites. Besides ON bipolar cells we also examined if OFF bipolar cells contributed to conglomerate forming population 3 Cx36 plaques by utilizing an antiserum against AMPA-type glutamate receptor subunit-4 (GluA4N). It is controversial if kainate or AMPA glutamate receptors are the main contributors to transmit signals from cones to OFF bipolar

cells. However, it has been shown that GluA4N is expressed by OFF bipolar cells in the primate and ground squirrel retina (Haverkamp et al. 2001; DeVries et al. 2006; Li and DeVries 2006), thus we can utilize GluA4N as a marker for OFF bipolar cell dendritic tips. We found that GluA4N plaques formed loose aggregates in the human OPL (Fig. 6k–m). When this staining was compared to Cx36 labels it was evident that the GluA4N and Cx36 plaques occupied similar subpedicle positions. Furthermore, individual Cx36 plaques were often found in the immediate vicinity of small GluA4N plaques. This suggested that both ON and OFF bipolar cell dendritic tips contributed to the population 3 Cx36 conglomerate formation.

Cx36 conglomerates are formed by BC dendritic tips

The shape and location of conglomerates strongly resembled Cx36 GJs formed by dendritic tips of OFF cone BCs in the mouse (Feigenspan et al. 2004) and the macaque retina (O'Brien et al. 2012). In order to prove the similar origin of the observed human Cx36 conglomerates (population 3), we carried out multiple label immunohistochemical reactions with known BC markers and Cx36. Recoverin (Rec) and CaB were selected to detect subpopulations of cone BCs, whereas the antibody against protein kinase $\text{C}\alpha$ ($\text{PKC}\alpha$) was used as a rod BC marker (Haverkamp et al. 2003). Rod BCs served as negative controls in this study as they have never been shown to be tracer-coupled, to form GJs or to express Cx proteins (Feigenspan et al. 2004).

$\text{PKC}\alpha$

It has been shown that $\text{PKC}\alpha$ is selectively expressed by rod BCs in retinas of non-primate mammals (Greferath et al. 1990), in macaques (Grünert et al. 1994) and humans (Haverkamp et al. 2003). Besides rod BCs, $\text{PKC}\alpha$ is also expressed to a lesser extent by DB4 invaginating ON BCs in all primates. We found that the $\text{PKC}\alpha$ antibody selectively labeled a subpopulation of BCs that displayed characteristics of rod BCs, including short tufted dendrites in the OPL, a short dendritic stalk, a round soma typically located in the distal half of the INL and long axonal processes that formed lobular axonal endings in the innermost stratum (stratum 5) of the IPL (Fig. 7a). As expected, dendrites of $\text{PKC}\alpha$ positive rod BCs showed no evidence of significant colocalization with Cx36 punctate labels in the OPL. Clearly, rod BC dendritic tips ended in an OPL sublayer distal to the location of conglomerates, and showed co-localizations only rarely with solitary Cx36 plaques (Fig. 7b–d).

Recoverin

A population of primate OFF/flat midget BCs with cell bodies in the mid-INL, a single long and thick dendritic stalk and an axon that terminated broadly in the OFF sublamina of the IPL has been reported to show Rec immunoreactivity (Milam et al. 1993; Wässle et al. 1994; Haverkamp et al. 2003). The Rec antiserum utilized in this study recognized a similar subset of BCs (Fig. 8a, b). Although, the intensive Rec immunoreactivity (Rec⁺) of photoreceptors obscured some of the BC dendritic labels, Rec⁺ dendrites were regularly observed and traced to their very tip. The Rec/Cx36 dual staining revealed Cx36 plaques that were clearly associated with Rec⁺ BC dendrites. We found co-localizations between Rec⁺ dendritic tips and conglomerate forming Cx36 plaques (population 3) as well as between dendritic branches and population 4 solitary plaques (Fig. 8c–f). To validate co-localizations, a thorough image analysis in Z-stacks of the Rec/Cx36

material was performed on randomly (the red color channel was turned off) selected Cx36 plaques ($n = 150$). In fact, we found that many examined Cx36 plaques ($n = 34$, 22.7 %) showed intensity maximums that correlated with overlapping Rec⁺ structures (Fig. 8d–g) as a sign of true co-localizations between the Cx36 and Rec stainings. Furthermore, many (14 out of 34) Rec⁺ structures were identified as Rec⁺ BC dendritic tips that colocalized with conglomerate Cx36 plaques. Therefore, Rec⁺ OFF cone BC dendrites clearly contributed to these structures. However, it was also clear that the majority of the conglomerate forming Cx36 plaques were Rec negative, and thus they were expressed by other neuron populations. Besides conglomerates, a number of Rec/Cx36 co-localizations (7 out of 34) were formed by Cx36 plaques that belonged to the proximal solitary plaque population (population 4). These latter Cx36 plaques did not occupy dendritic tips, but rather localized on thicker preterminal branches of Rec⁺ BCs. The remaining

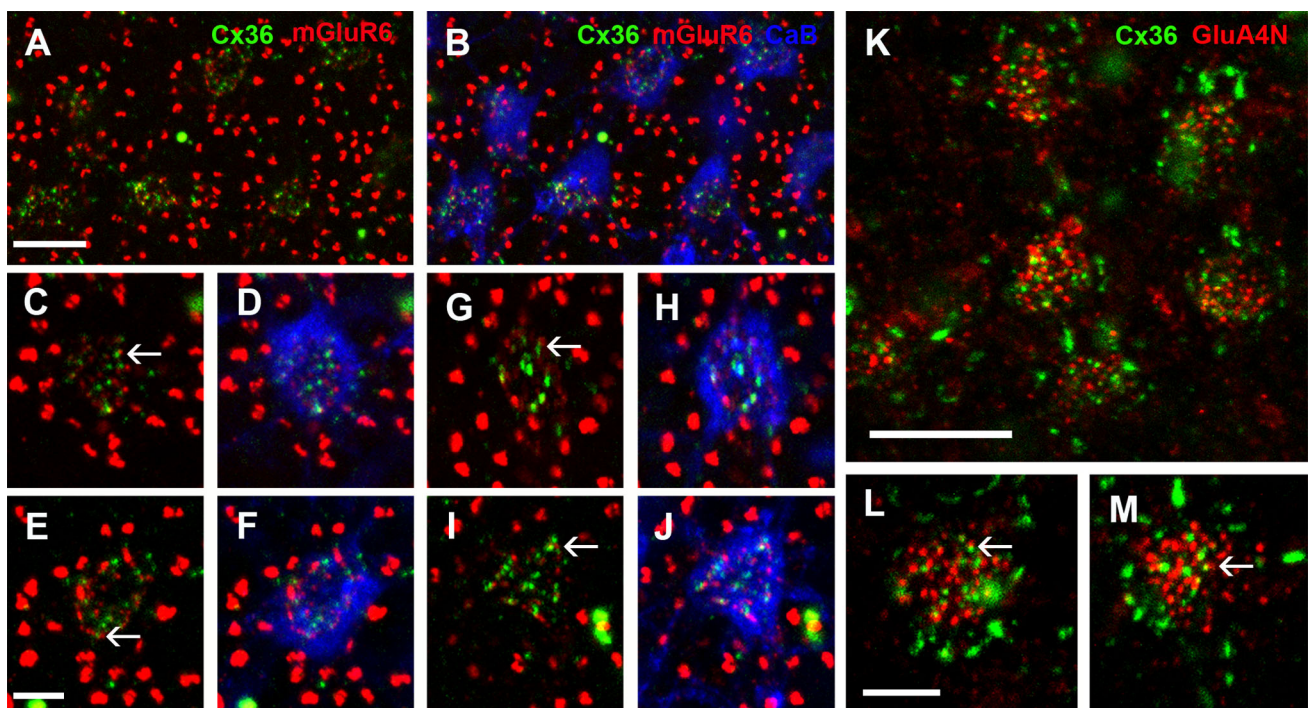


Fig. 6 Subpedicle Cx36 plaques are strongly associated with postsynaptic glutamate receptors. **a** Photomicrograph showing mGluR6 (red) and Cx36 (green) immunoreactivity in a whole-mount specimen of the human OPL from midperipheral location. The mGluR6 immunoreactive label showed larger structures (likely duplexes or triplexes of rod bipolar dendrites) in OPL regions that harbored relatively few population 2 Cx36 plaques and also displayed aggregates of smaller immunoreactive population 3 Cx36 dots. The aggregates of these latter small mGluR6 labels were intermingled with the subpedicle Cx36 conglomerates. **b** This image shows the same frame as in **a** with CaB (blue) counterlabels to stain cone pedicles. Clearly, larger mGluR6 spots were in cone pedicle exclusion

zones, whereas intermingled small mGluR6 and Cx36 plaques occurred strictly in subpedicle areas. **c–j** Magnified image pairs (**c–d**, **e–f**, **g–h**, **i–j**) show individual cone pedicles with strongly associated mGluR6 and Cx36 plaques (arrows). **k–m** Photomicrographs are showing the human OPL in a whole-mount specimen with GluA4N (red) and Cx36 (green) immunoreactivity. GluA4N label was readily found among Cx36 plaques of subpedicle conglomerates (**k**). Many GluA4N plaques showed a strong steric association with conglomerate forming Cx36 plaques (arrows in **l**, **m**). All images show MIPs of five optical sections (5 \times , 250 nm). Scale bar 10 μ m on **a** and **k** and 5 μ m for **c–j** and **l–m**

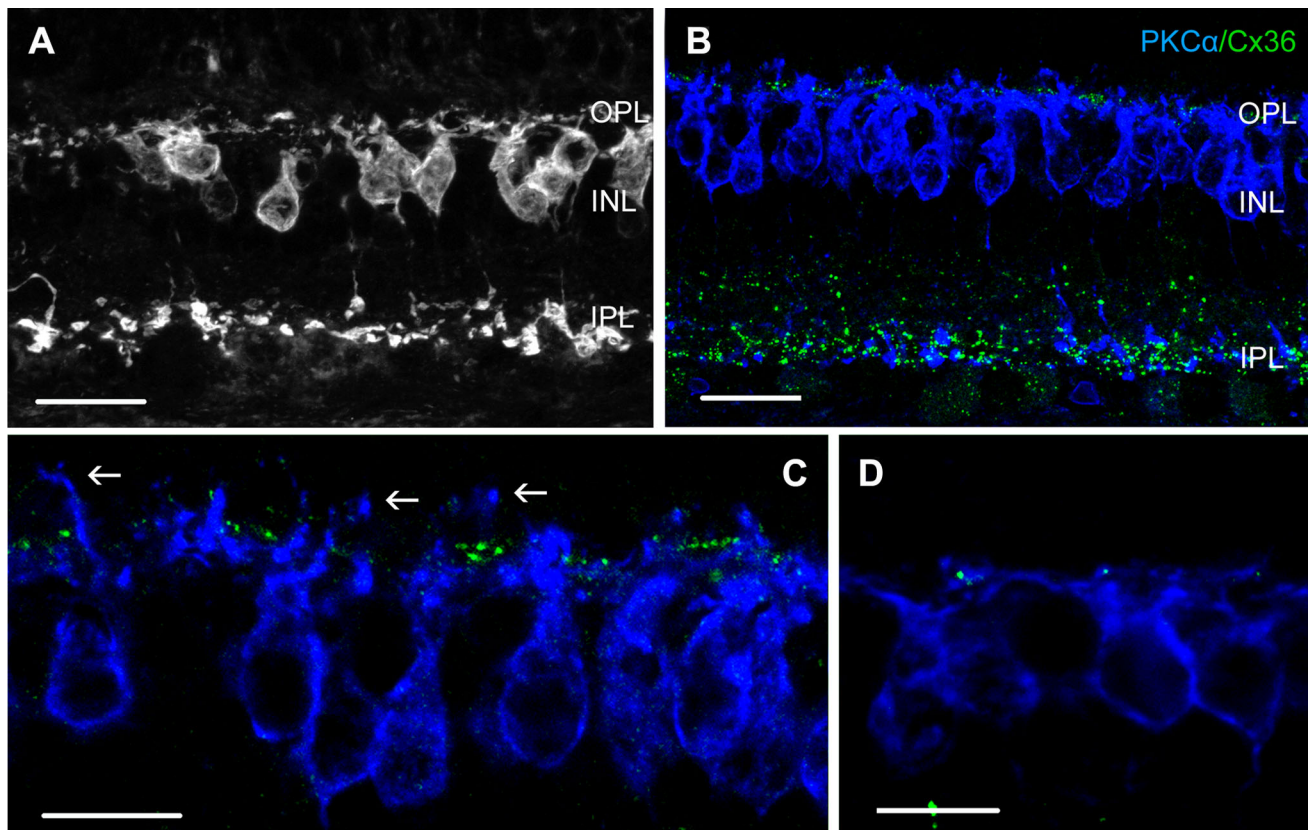


Fig. 7 Cx36 plaques do not colocalize with dendritic tips of rod bipolar cells. **a** An antiserum against PKC α revealed a subset of bipolar cells with distally located cell bodies, short dendritic tufts and small dendritic fields, as well as long vertically running axons that arborized in the innermost strata of the IPL and showed lobular endings. This architecture of labeled bipolar cells corresponded to those of rod bipolar cells in mammalian species. **b** Dendritic tips of rod bipolar cells (*blue*) ended distal to OPL substrata that contained

examined Rec/Cx36 co-localizations belonged to Rec $^{+}$ photoreceptor pedicles.

Calbindin-D28

The 28 kDa calcium binding buffer protein CaB has been shown to be expressed in cones, HCs, a subset of amacrine cells and two types of BCs in non-primate mammals (Massey and Mills 1996; Völgyi et al. 1997), in macaques (Grünert et al. 1994) and in humans (Haverkamp et al. 2003). In primates, CaB is expressed by DB3 flat diffuse OFF cone BCs. Here, we found that the anti-CaB serum labeled cone photoreceptors, HCs and subsets of BC, amacrine and ganglion cells (Fig. 9a, b). The labeled BCs had several thin dendritic branches that arborized widely and contacted multiple neighbouring cones, their somata were located in the middle of the INL and their axons entered the IPL. The stratification level of the CaB $^{+}$ BC axon terminals could not be visualized clearly due to the dense CaB $^{+}$ plexus of other inner retinal neurons.

both solitary Cx36 plaques (*green*) and Cx36 conglomerates. Axonal endings of rod bipolar cells on the other hand, showed a close approximation to strata where the density of Cx36 plaques was the highest. **c, d** High magnification view showing that both populations of Cx36 plaques generally avoid rod bipolar cell dendritic tips (**c**; *arrows*). Images in **a–c** are projections of five consecutive 0.5 μ m thick optical sections, whereas **d** is a single optical section. *Scale bar* 10 μ m

Similarly, the CaB $^{+}$ BC dendrites in the OPL could not always be followed all the way to the tips due to the close proximity of the CaB $^{+}$ HC processes. However, we were able to track some CaB $^{+}$ BC dendrites that displayed population 3, conglomerate forming Cx36 plaques located on their tips (Fig. 9c–j). In addition, we also observed many solitary, population 4 Cx36 plaques that were associated with CaB $^{+}$ BC dendritic branches. We performed Z-stack image analysis in randomly selected plaques ($n = 200$) in the CaB/Cx36 stained specimen. This confirmed that many Cx36 plaques (50 out of 200; 25 %) showed Z-scale intensity maximums that overlapped with those of the CaB $^{+}$ structures (Fig. 9f–h). When colocalizing CaB $^{+}$ structures were traced back to their origin, they appeared as cone pedicles ($n = 15$), BC dendritic tips ($n = 18$) or BC preterminal dendrites ($n = 17$). Therefore, similar to Rec $^{+}$ BCs, CaB $^{+}$ BC dendritic tips also expressed Cx36 plaques that contributed to conglomerates (population 3 plaques). Moreover, CaB $^{+}$ preterminal BC dendrites colocalized with proximal solitary, population 4

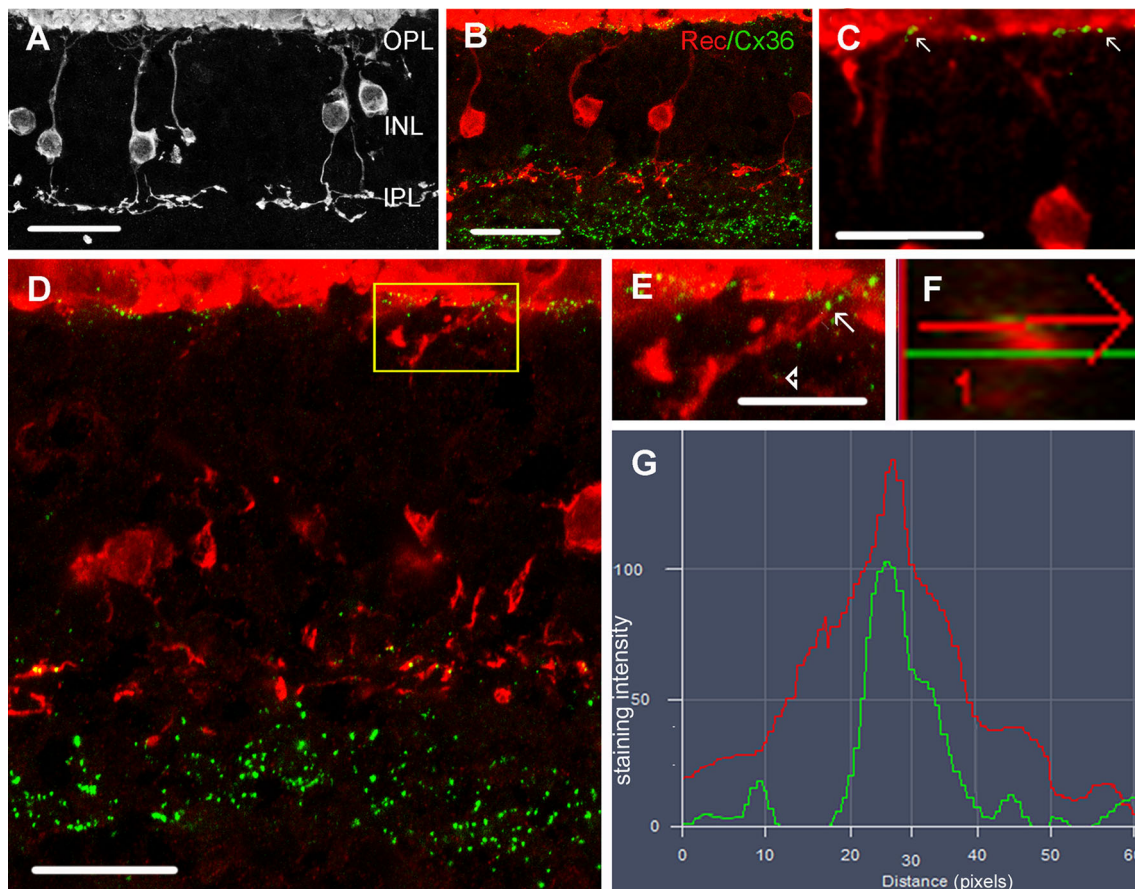


Fig. 8 Cx36 plaques colocalize with dendritic tips of recoverin-expressing bipolar cells. **a** The anti-Rec antiserum specifically labels a population of OFF cone bipolar cells with somata in the middle of the INL and axon terminals stratifying in stratum 1 and 2 of the IPL. **b** Both dendrites in the OPL and axons in the IPL of Rec⁺ bipolar cells (red) appeared to co-stratify with Cx36 plaques (green). **c** Cx36 plaques that were located on dendritic tips of Rec⁺ OFF cone bipolar cells appeared to contribute to population 3 subpedicle conglomerates (arrows). **d–g** Rec/Cx36 Z-stacks (**d**, **e**) were processed to generate

orthogonal views of putative colocalizing Cx36 plaques (**f**). The maximum intensity of the two stainings overlapped considerably (**g**) confirming the colocalization. Arrow in **e** shows population 3 Cx36 plaque that colocalizes with a Rec⁺ dendritic tip, whereas the arrowhead displays the colocalization of a labeled dendritic branch and a solitary population 4 Cx36 plaque. **a**, **b** MIPs of 27 optical sections (27 × 250 nm), **c–e** display MIPs of 5 optical sections (5 × 250 nm). Scale bar 20 μm in **a–d**, 10 μm in **e** and **f**

plaques (Fig. 9i, j). Very rarely, we also found Cx36 plaques that colocalized with HC processes or were situated at crossings of CaB⁺ HC processes and unidentified CaB stained fibers (Fig. 9k).

Discussion

Cx36 has been reported to form GJs in the outer retina in a number of mammalian species (Güldenagel et al. 2000, 2001; Feigenspan et al. 2004; Deans et al. 2002; Mills et al. 2001; Bloomfield and Völgyi 2009; Völgyi et al. 2013a). The sole available study on human retina by Söhl and colleagues (2010) reported the presence of Cx36 in the human outer retina as well, although the identity of the GJ forming neuronal components was not determined. In this study, we performed an

elaborate immunohistochemical survey by using well-preserved human material to examine the expression and the spatial distribution of Cx36 in the outer retina and to delineate the corresponding neuronal circuits. The exceptional quality of the presented material allowed the characterization of Cx36-forming circuit elements of the human outer retina, a task that has previously been challenging. We found that similar to other species, Cx36 GJs connect cones into spatially confined arrays, underlie cone-to-rod coupling and connect cone BC dendrites to one another.

Four populations of Cx36 plaques exist in the human OPL

Based on their locations in the OPL, we identified four populations of Cx36 plaques in the human retina (Table 2):

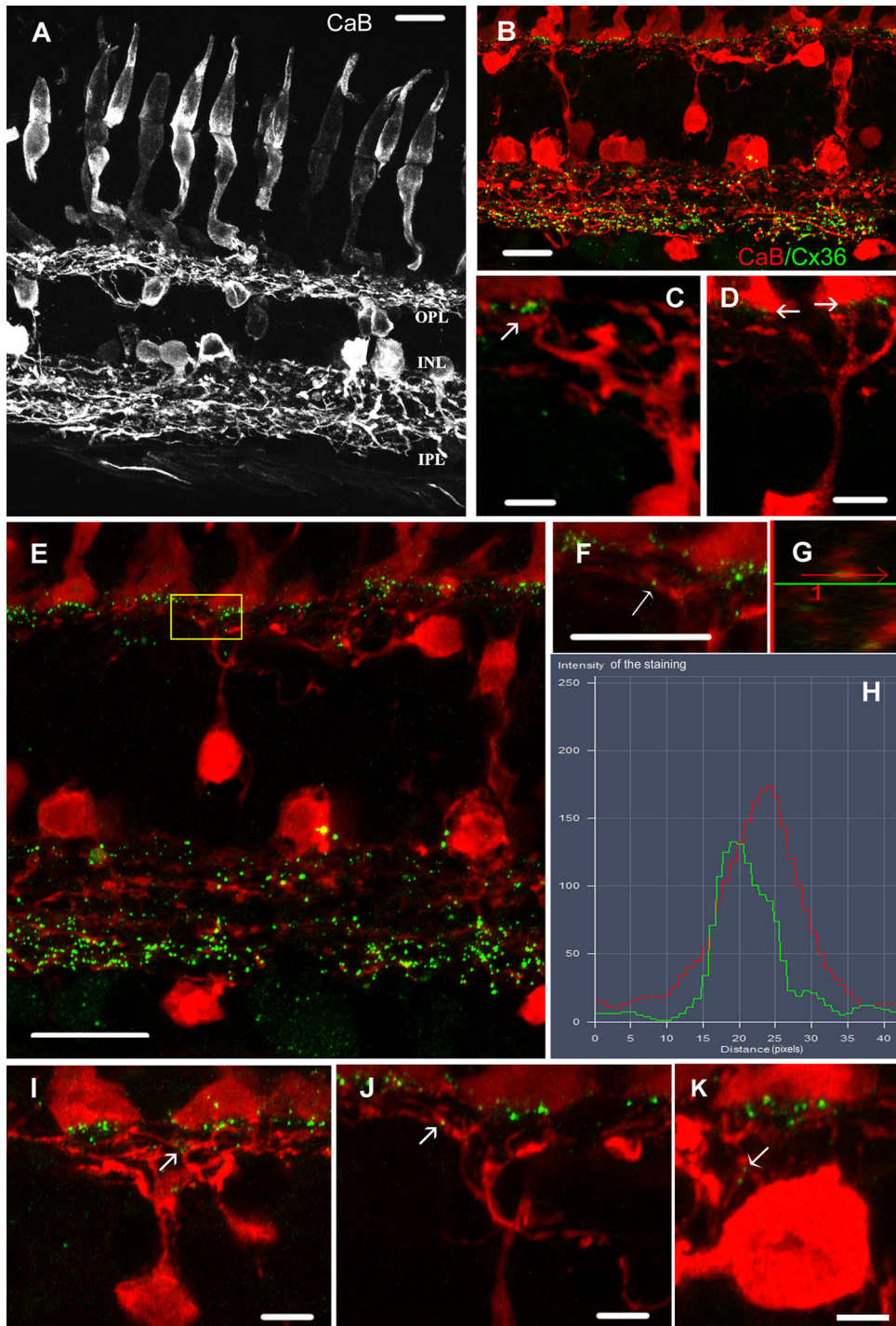


Fig. 9 Cx36 plaques colocalize with dendritic tips of calbindin expressing bipolar cells. **a** An overview of CaB immunolabeling in the central human retina shows CaB positivity in cone photoreceptors, horizontal cells, one or two subpopulations of bipolar cells with widely arborizing dendritic tree in the OPL and a mixed population of amacrine and ganglion cells in the inner retina. **b** CaB⁺ bipolar cells (red) possess dendrites that protrude towards subpedicle conglomerates and intermingle with Cx36 (green) plaques in the OPL. **c, d** High magnification views of CaB⁺ bipolar cell dendrites colocalized with Cx36 plaques that contribute to population 3, Cx36 conglomerates in the OPL (arrows). **e–h** CaB/Cx36 Z-stacks (**e, f**) were processed to generate orthogonal views of putative colocalizing Cx36 plaques (**g**). Rectangle in **e** marks enlarged area of **f** with a population 4 Cx36 plaque (arrow) analyzed further in **g** and **h**. The maximum intensity of the two stainings overlapped considerably (**h**) confirming the colocalization. **i–k** Occasionally we found Cx36 plaques at crossings of horizontal cell dendrites (**k**), whereas population 4 Cx36 plaques were found more often in CaB⁺ bipolar cell dendritic crossings (arrows in **i, j**). Besides population 4 plaques, CaB⁺ dendritic tips harbored some population 3 conglomerate forming Cx36 plaques as well. **a, b** MIPs of 19 optical sections (19×, 250 nm), **c–k** are MIPs of 4–6 optical sections (4–6×, 250 nm). Scale bar 20 μm in **a, b** and **e**, 10 μm in **f, g** and 5 μm in **c, d, i, j** and **k**

(1) population 1 solitary plaques occurred distally and often colocalized with M/L cones; (2) population 2 solitary plaques were located at the level of cone pedicles and often colocalized with pedicles or even found in pedicle contacts; (3) population 3 Cx36 plaques formed densely packed conglomerates in subpedicle locations and colocalized with dendritic tips that were visualized with bipolar cell markers and (4) scattered population 4 Cx36 plaques were found in the proximalmost aspect of the OPL and often colocalized with bipolar cell markers. Figure 10b shows the plaques that were sorted and colorcoded according to this above characterization scheme. The above sections of this study detailed experiments designed to identify the neuronal elements that harbor Cx36 plaques of each population and the following paragraphs will summarize our findings in the light of previous results.

Cx36 GJs mediate photoreceptor coupling

Cones have been shown to express Cx36 in various mammals including the monkey, rabbit, mouse, guinea pig (Raviola and Gilula 1973; Deans et al. 2002; Feigenspan et al. 2004; Lee et al. 2003; O'Brien et al. 2012) and humans (Söhl et al. 2010). Some of these contacts have been shown to be functional GJs that allow for the electrical and tracer coupling of nearby cones (Schneeweis and Schnapf 1999; Li and DeVries 2004). It appears that this Cx36 GJ-mediated coupling is generally present between spectrally identical cones. In addition, spectrally indiscriminate coupling has also been reported between trichromate primate L and M cones, but not S cones

(Hornstein et al. 2004). Population 1 and 2 solitary Cx36 plaques in our study were also associated with L and M cone photoreceptor terminals, whereas conglomerates and proximal solitary Cx36 plaques (population 3 and 4) were clearly too far to partake in such photoreceptor coupling. In fact, population 1 and more typically population 2 solitary Cx36 plaques were often found at sites of intimate cone terminal contacts indicating that they were sites of functional cone-to-cone GJs. However, the antiserum labeled both M and L cones, and therefore we could not differentiate between spectrally discriminative and indiscriminate GJs. Overall, these findings indicate that, similar to other mammals, cones of the human retina utilize Cx36 GJs to increase the signal-to-noise ratio of cone-mediated signaling (Bloomfield and Völgyi 2009; Völgyi et al. 2013a).

Similar to M/L-cones, S-cones also expressed solitary Cx36 plaques on their axonal terminals but due to the low S-cone frequency solitary Cx36 plaques were not observed at contact sites of nearby S-cones. On the other hand, S-cones theoretically could form GJs with nearby M/L-cones, whose close proximity allows for direct physical contacts. Although, we can not entirely rule this out, such spectrally indiscriminate coupling of M/L-cones with S-cones has not been found in trichromate monkeys (Hornstein et al. 2004), and it likely does not exist in the human retina either. In addition, rod-to-cone GJs could also account for the observed colocalization of solitary Cx36 plaques and S-cone terminals.

A number of solitary Cx36 plaques were colocalized with single M/L-cone pedicles and we first hypothesized that these were possible sites of rod-to-cone GJs (Bloomfield and Völgyi 2009; Völgyi et al. 2013a). In fact, we found the presence of population 1 and 2 Cx36 plaques in a number of rod-to-cone contact sites in both Cx36/PNA/rTR and Cx36/CaB/rTR stainings as a strong support for this hypothesis. The role of Cx36 GJs in such contacts has been described as the bottle-neck of the secondary rod pathway in a variety of mammals (Lee et al. 2003; Güldenagel et al. 2001; Feigenspan et al. 2001; Deans et al. 2002) and psychophysical evidence suggested the functionality of this pathway in humans (Sharpe and Stockman 1999). Therefore, our results indicate that the observed Cx36 GJs in rod-to-cone contacts might serve the secondary rod pathway in humans. Besides plaques in rod-to-cone contacts, we found Cx36 plaques that were located at sites of neighboring rod spherule appositions. This suggests that rods also express Cx36 in their hemichannel and that Cx36 GJs might form rod-to-rod contacts as well. This finding apparently contradicts to previous results in mice where rods do not express Cx36 (Feigenspan et al. 2004), thus our hypothesis needs further experimental support.

Strategic positioning of Cx36 GJs may serve distinct BC functions

Both population 4 solitary Cx36 plaques and plaques that formed disc-like conglomerates beneath cone pedicles (population 3) were observed in locations that suggested their BC origin. Single cell reverse transcriptase PCR showed that HCs and rod BCs do not express Cx36, and thus do not contribute to the characteristic Cx36 label in the mouse OPL (Feigenspan et al. 2004). In this study, we found no significant colocalization between rod BC dendrites and Cx36 plaques either. The rarely seen overlap between Cx36 plaques and PKC α labeled processes can be accounted for the combination of mere chance and the PKC α -stained DB4 ON BCs (Grünert et al. 1994;

Haverkamp et al. 2003). Söhl and colleagues (2010) showed that HCs of the human retina express Cx59 and Cx62 (human orthologues of the mouse Cx57) and not Cx36. The occasional Cx36 plaques that appeared to colocalize with human HC processes in this study were rather rare and did not seem significant compared to the high number of Cx36 plaques and the prevalence of HC dendrites. This indicated that conglomerate forming population 3 Cx36 plaques and population 4 solitary plaques interconnect cone BCs, and are not associated with either HCs or rod BCs.

A mixed population of OFF cone BCs have been shown responsible for Cx36 conglomerates in the mouse and the primate retina (Feigenspan et al. 2004; O'Brien et al. 2012). In this work, we found that population 3 Cx36

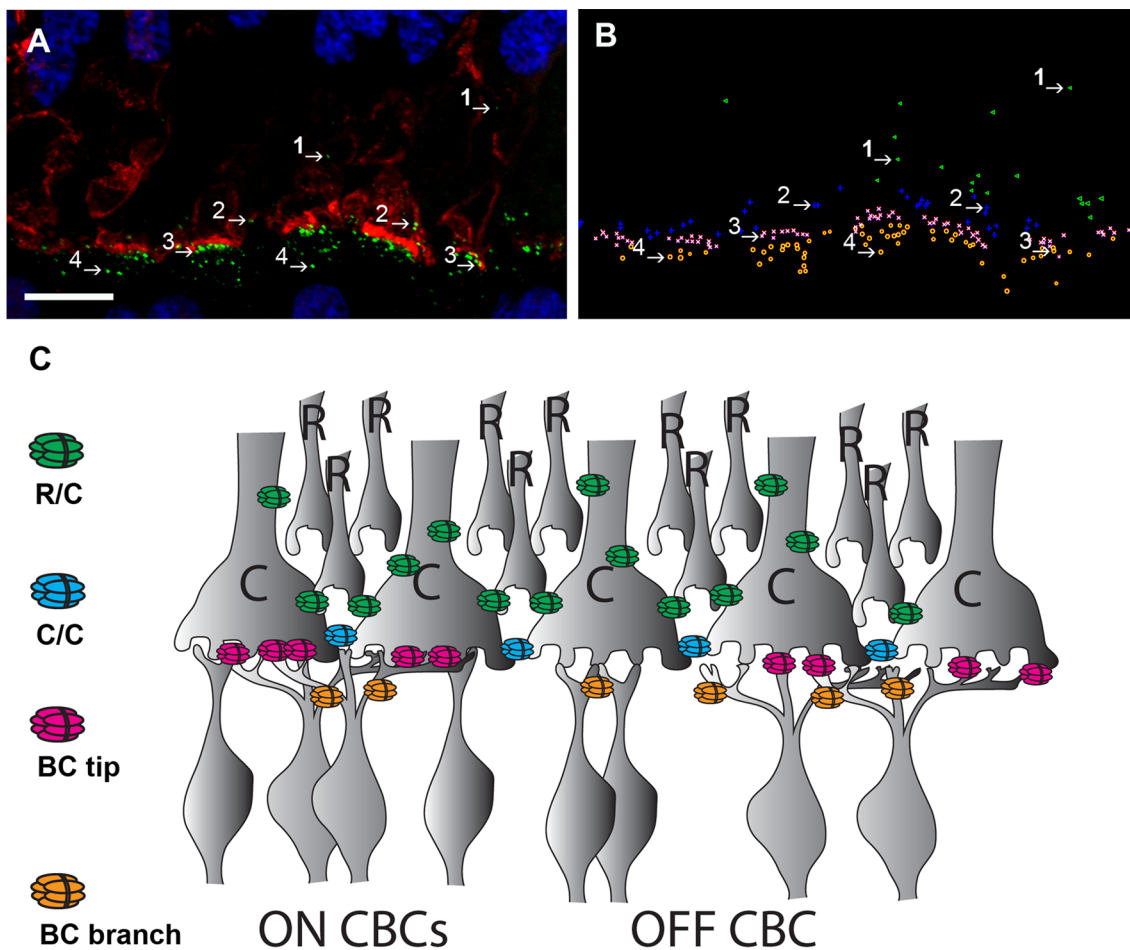


Fig. 10 Four populations of Cx36 plaques exist in the human OPL. **a** Photomicrograph showing MIPs of 28 optical sections (28×250 nm) of a triple stained radial section of the human OPL that visualize nuclei in the ONL and distal INL (DAPI—blue), M/L cones (red) and Cx36 plaques (green). Four populations of Cx36 plaques (1, 2, 3 and 4; also see text) are clearly visible in this section. **b** Neurolucida mapping from the same area of the section in **a** colorcodes individual Cx36 plaques of the four populations;

population 1—green, population 2—blue, population 3—magenta, population 4—orange. **c** Summary drawing presents the suggested cellular contacts (based on results of this paper) served by Cx36 plaques in each of the four populations. *R* rod, *C* cone, *BC* bipolar cell, *ON CBC* ON center cone bipolar cell, *OFF CBC* OFF center cone bipolar cell, colored hexameric structures represent Cx36 GJs. Scale bar 10 μ m

conglomerates were arranged in a regular honey-comb pattern and occupied subpedicle spaces of both M/L- and S-cones. Further examination showed that the Cx36 density was uniform across the entire conglomerate population, thus suggesting that the two subpopulations (M/L- and S-cone associated) only differed in the area size but not in the density of the Cx36-expressing neuronal structures. Our double-labeling experiments confirmed that the Rec⁺ and CaB⁺ subpopulations of OFF BCs in the human retina contributed to the observed population 3 Cx36 conglomerates. In both cases, we tracked representative BC dendrites from their somatic origin all the way to the very tip, where colocalizing Cx36 plaques were discernible. This observation indicates that conglomerates in the human retina, similar to mice (Feigenspan et al. 2004), are sites of Cx36 GJs formed between cone BC dendritic tips. However, it was evident that CaB⁺ and Rec⁺ dendrites expressed only a fraction of the conglomerate plaques, and thus indicated that further BC populations participate in this characteristic contact. In fact, neurokinin-3 receptor and HCN4 potassium channel expressing BCs in mouse and glutamate transporter (GLT-1) expressing BCs in the monkey have been shown to contribute to Cx36 conglomerates (Feigenspan et al. 2004; O'Brien et al. 2012). This observation, therefore, indicates that conglomerate GJs serve to connect various cone BC types that share the same presynaptic photoreceptor.

Population 4 Cx36 plaques were sparse, solitary and connected thicker preterminal branches of neighbour BCs in both the Rec and the CaB experiments. This pattern was distinguishable from the densely packed conglomerate forming population 3 Cx36 plaques that appeared in BC dendritic tips. We speculate that the distinct positioning of population 3 and 4 BC GJ populations serve different roles in visual signal transmission. The subpedicle location and the shape of conglomerates resembled aggregations of glutamate and/or GABA receptors localized on BC and HC dendritic tips (Haverkamp et al. 2000, 2001; O'Brien et al. 2012). In fact, we showed the close association of population 3 conglomerate forming Cx36 plaques with mGluR6 and GluA4N postsynaptic glutamate receptors that occur in dendritic tips of ON and OFF cone bipolar cells, respectively. This further indicates that similar to postsynaptic glutamate receptors, population 3 Cx36 plaques are expressed by BC dendritic tips. Furthermore, the juxtaposition of Cx36 plaques and postsynaptic glutamate receptors strongly suggests their functional correlation as well. For example, changes in the GJ conductance might modify the postsynaptic efficacy of chemical synaptic transmission. On the other hand, population 4 solitary Cx36 plaques were relative far from these glutamatergic synaptic sites. Thus, population 4 solitary BC GJs are rather positioned to correlate signals of nearby BCs rather than modify

chemical synaptic signaling. This suggests a dichotomy in GJ signaling between BCs. In this scenario, population 3 Cx36 GJs distributes signals across BCs that share the same presynaptic cone and perhaps alter the efficacy of photoreceptor inputs. Contrary, population 4 Cx36 GJs likely correlates signals of nearby BCs with inputs from different photoreceptors. Overall, we found that the distribution of Cx36 plaques in the human outer retina shows similarities to those described in other mammalian models. Furthermore, the presented work revealed the wealth of Cx36 GJs in the first synaptic layer of the human retina and pointed out their functional diversity.

Acknowledgments The authors thank to Zsuzsanna Vidra for her technical help and are grateful to Dr. Mark Eyre for the assistance with the English language. The authors are thankful for providing the antibodies: Noga Vardi (mGluR6), Wilhelm Koch (recoverin), Alán Alpár (guinea pig calbindin), Norbert Hájos (GluA4N). Supported by OTKA K105247 to B.V. and OTKA 73000 Á.S. This research was supported by the European Union and the State of Hungary, co-financed by the European Social Fund in the framework of TÁMOP-4.2.4.A/2-11/1-2012-0001 'National Excellence Program' to B.V. Finally, B.V. was also supported by the Hungarian Brain Research Program (KTIA_NAP_13-2-2015-0008).

Compliance with ethical standards

Conflict of interest The authors declare that they have no conflict of interest.

Ethical standards All procedures performed in studies involving human participants were in accordance with the ethical standards of the institutional research committee (number of permission: TUKEB 58/2006) and with the 1964 Helsinki declaration and its later amendments.

References

- Ahnelt P, Kolb H (1994) Horizontal cells and cone photoreceptors in human retina: a Golgi-electron microscopic study of spectral connectivity. *J Comp Neurol* 343:406–427
- Ahnelt PK, Kolb H, Pflug R (1987) Identification of a subtype of cone photoreceptor, likely to be blue sensitive, in the human retina. *J Comp Neurol* 255:18–34
- Ahnelt PK, Keri C, Kolb H (1990) Identification of pedicles of putative blue sensitive cones in human and primate retina. *J Comp Neurol* 293:39–53
- Bloomfield SA, Völgyi B (2009) The diverse functional roles and regulation of neuronal gap junctions in the retina. *Nat Rev Neurosci* 10:495–506. doi:10.1038/nrn2636
- Bumsted K, Hendrickson A (1999) Distribution and development of short-wavelength cones differ between Macaca monkey and human fovea. *J Comp Neurol* 403:502–516
- Cruciani V, Mikalsen SO (2006) The vertebrate connexin family. *Cell Mol Life Sci* 63:1125–1140
- Deans MR, Völgyi B, Goodenough DA, Bloomfield SA, Paul DL (2002) Connexin36 is essential for transmission of rod-mediated visual signals in the mammalian retina. *Neuron* 36:703–712
- DeVries SH, Li W, Saszik S (2006) Parallel processing in two transmitter microenvironments at the cone photoreceptor synapse. *Neuron* 50:735–748

- Feigenspan A, Teubner B, Willecke K, Weiler R (2001) Expression of neuronal connexin36 in AII amacrine cells of the mammalian retina. *J Neurosci* 21:230–239
- Feigenspan A, Janssen-Bienhold U, Hormuzdi S, Monyer H, Degen J, Söhl G, Willecke K, Ammermüller J, Weiler R (2004) Expression of connexin36 in cone pedicles and OFF-cone bipolar cells of the mouse retina. *J Neurosci* 24:3325–3334
- Furshpan EJ, Potter DD (1957) Mechanism of nerve-impulse transmission at a crayfish synapse. *Nature* 180:342–343
- Greferath U, Grünert U, Wässle H (1990) Rod bipolar cells in the mammalian retina show protein kinase C-like immunoreactivity. *J Comp Neurol* 301:433–442
- Grünert U, Martin PR, Wässle H (1994) Immunocytochemical analysis of bipolar cells in the macaque monkey retina. *J Comp Neurol* 348:607–627
- Güldenagel M, Söhl G, Plum A, Traub O, Teubner B, Weiler R, Willecke KS (2000) Expression patterns of connexin genes in mouse retina. *J Comp Neurol* 425:193–201
- Güldenagel M, Ammermüller J, Feigenspan A, Teubner B, Degen J, Söhl G, Willecke K, Weiler R (2001) Visual transmission deficits in mice with targeted disruption of the gap junction gene connexin36. *J Neurosci* 21:6036–6044
- Han Y, Massey SC (2005) Electrical synapses in retinal ON cone bipolar cells: subtype-specific expression of connexins. *Proc Natl Acad Sci USA* 102:13313–13318
- Haverkamp S, Grünert U, Wässle H (2000) The cone pedicle, a complex synapse in the retina. *Neuron* 27:85–95
- Haverkamp S, Grünert U, Wässle H (2001) The synaptic architecture of AMPA receptors at the cone pedicle of the primate retina. *J Neurosci* 21:2488–2500
- Haverkamp S, Haeseleer F, Hendrickson A (2003) A comparison of immunocytochemical markers to identify bipolar cell types in human and monkey retina. *Visual Neurosci* 20:589–600
- Hendrickson A, Yan YH, Erickson A, Possin D, Pow D (2007) Expression patterns of calretinin, calbindin and parvalbumin and their colocalization in neurons during development of Macaca monkey retina. *Exp Eye Res* 85:587–601
- Hidaka S, Akahori Y, Kurosawa Y (2004) Dendrodendritic electrical synapses between mammalian retinal ganglion cells. *J Neurosci* 24:10553–10567
- Hombach S, Janssen-Bienhold U, Söhl G, Schubert T, Büssov H, Ott T, Weiler R, Willecke K (2004) Functional expression of connexin57 in horizontal cells of the mouse retina. *Eur J Neurosci* 19:2633–2640
- Hornstein EP, Verweij J, Schnapf JL (2004) Electrical coupling between red and green cones in primate retina. *Nat Neurosci* 7:745–750
- Hunyady B, Krempels K, Harta G, Mezey E (1996) Immunohistochemical signal amplification by catalyzed reporter deposition and its application in double immunostaining. *J Histochem Cytochem* 44:1353–1362
- Kántor O, Temel Y, Holzmann C, Raber K, Nguyen HP, Cao C, Türkoglu HO, Rutten BP, Visser-Vandewalle V, Steinbusch HW et al (2006) Selective striatal neuron loss and alterations in behavior correlate with impaired striatal function in Huntington's disease transgenic rats. *Neurobiol Dis* 22:538–547
- Kihara AH, Mantovani de Castro L, Belmonte MA, Yan CY, Moriscot AS, Hamassaki DE (2006) Expression of connexins 36, 43, and 45 during postnatal development of the mouse retina. *J Neurobiol* 66:1397–1410
- Kihara AH, Santos TO, Osuna-Melo EJ, Paschon V, Vidal KS, Akamine PS, Castro LM, Resende RR, Hamassaki DE, Britto LR (2010) Connexin-mediated communication controls cell proliferation and is essential in retinal histogenesis. *Int J Dev Neurosci* 28:39–52. doi:10.1016/j.ijdevneu.2009.09.006
- Kolb H, Goede P, Roberts S, McDermott R, Gouras P (1997) Uniqueness of the S-cone pedicle in the human retina and consequences for color processing. *J Comp Neurol* 386:443–460
- Kovács-Öller T, Raics K, Orbán J, Nyitrai M, Völgyi B (2014) Developmental changes in the expression level of connexin36 in the rat retina. *Cell Tissue Res* 358:289–302. doi:10.1007/s00441-014-1967-9
- Lee EJ, Han JW, Kim HJ, Kim IB, Lee MY, Oh SJ, Chung JW, Chun MH (2003) The immunocytochemical localization of connexin 36 at rod and cone gap junctions in the guinea pig retina. *Eur J Neurosci* 18:2925–2934
- Li W, DeVries SH (2004) Separate blue and green cone networks in the mammalian retina. *Nat Neurosci* 7:751–756
- Li W, DeVries SH (2006) Bipolar cell pathways for color and luminance vision in a dichromatic mammalian retina. *Nat Neurosci* 9:669–675
- Lin B, Jakobs TC, Masland RH (2005) Different functional types of bipolar cells use different gap-junctional proteins. *J Neurosci* 25:6696–6701
- Massey SC, Mills SL (1996) A calbindin-immunoreactive cone bipolar cell type in the rabbit retina. *J Comp Neurol* 366:15–33
- Massey SC, O'Brien JJ, Trexler EB, Li W, Keung JW, Mills SL, O'Brien J (2003) Multiple neuronal connexins in the mammalian retina. *Cell Commun Adhes* 10:425–430
- Maxeiner S, Dedek K, Janssen-Bienhold U, Ammermüller J, Brune H, Kirsch T, Pieper M, Degen J, Krüger O, Willecke K et al (2005) Deletion of connexin45 in mouse retinal neurons disrupts the rod/cone signaling pathway between AII amacrine and ON cone bipolar cells and leads to impaired visual transmission. *J Neurosci* 25:566–576
- Milam AH, Dacey DM, Dizhoor AM (1993) Recoverin immunoreactivity in mammalian cone bipolar cells. *Visual Neurosci* 10:1–10
- Mills SL, O'Brien JJ, Li W, O'Brien J, Massey SC (2001) Rod pathways in the mammalian retina use connexin36. *J Comp Neurol* 436:336–350
- Müller LP, Dedek K, Janssen-Bienhold U, Meyer A, Kreuzberg MM, Lorenz S, Willecke K, Weiler R (2010) Expression and modulation of connexin 30.2, a novel gap junction protein in the mouse retina. *Vis Neurosci* 27:91–101. doi:10.1017/S0952523810000131
- Nathans J, Thomas D, Hogness D (1986) Molecular genetics of human color vision: the genes encoding blue, green and red pigments. *Science* 232:193–202
- O'Brien JJ, Chen X, Macleish PR, O'Brien J, Massey SC (2012) Photoreceptor coupling mediated by connexin36 in the primate retina. *J Neurosci* 32:4675–4687. doi:10.1523/JNEUROSCI.4749-11.2012
- Pan F, Paul DL, Bloomfield SA, Völgyi B (2010) Connexin36 is required for gap junctional coupling of most ganglion cell subtypes in the mouse retina. *J Comp Neurol* 518:911–927. doi:10.1002/cne.22254
- Pereda A, O'Brien JO, Nagy JI, Bukauskas F, Davidson KGV, Kamasawa N, Yasumura T, Rash JE (2003) Connexin35 mediates electrical transmission at mixed synapses on Mauthner cells. *J Neurosci* 23:7489–7503
- Petrasch-Parwez E, Habbes HW, Weickert S, Löbbbecke-Schumacher M, Striedinger K, Wiczorek S, Dermietzel R, Epplen JT (2004) Fine-structural analysis and connexin expression in the retina of a transgenic model of Huntington's disease. *J Comp Neurol* 479:181–197
- Rash JE, Kamasawa N, Davidson KGV, Yasumura T, Pereda AE, Nagy JI (2012) Connexin composition in apposed gap junction hemiplaques revealed by matched double-replica freeze-fracture replica immunogold labeling. *J Membr Biol* 245:333–344. doi:10.1007/s00232-012-9454-2

- Raviola E, Gilula NB (1973) Gap junctions between photoreceptor cells in the vertebrate retina. *Proc Natl Acad Sci USA* 70:1677–1681
- Sage D (2008) Watershed segmentation. Ecole Polytechnique Fédérale de Lausanne. <http://bigwww.epfl.ch/sage/soft/watershed>
- Schindelin J, Arganda-Carreras I, Frise E, Kaynig V, Longair M, Pietzsch T, Preibisch S, Rueden C, Saalfeld S, Schmid B et al (2012) Fiji: an open-source platform for biological-image analysis. *Nat Methods* 9:676–682. doi:10.1038/nmeth.2019
- Schneeweis DM, Schnapf JL (1999) The photovoltage of macaque cone photoreceptors: adaptation, noise, and kinetics. *J Neurosci* 19:1203–1216
- Schubert T, Degen J, Willecke K, Hormuzdi SG, Monyer H, Weiler R (2005a) Connexin36 mediates gap junctional coupling of alpha-ganglion cells in mouse retina. *J Comp Neurol* 485:191–201
- Schubert T, Maxeiner S, Krüger O, Willecke K, Weiler R (2005b) Connexin45 mediates gap junctional coupling of bistratified ganglion cells in the mouse retina. *J Comp Neurol* 490:29–39
- Sharpe LT, Stockman A (1999) Rod pathways: the importance of seeing nothing. *Trends Neurosci* 22:497–504
- Söhl G, Willecke K (2003) An update on connexin genes and their nomenclature in mouse and man. *Cell Commun Adhes* 10:173–180
- Söhl G, Jousseaume A, Kociok N, Willecke K (2010) Expression of connexin genes in the human retina. *BMC Ophthalmol* 10:27. doi:10.1186/1471-2415-10-27
- Völgyi B, Pollak E, Buzás P, Gábel R (1997) Calretinin in neurochemically well-defined cell populations of rabbit retina. *Brain Res* 763:79–86
- Völgyi B, Deans MR, Paul DL, Bloomfield SA (2004) Convergence and segregation of the multiple rod pathways in mammalian retina. *J Neurosci* 24:11182–11192
- Völgyi B, Abrams J, Paul DL, Bloomfield SA (2005) Morphology and tracer coupling pattern of alpha ganglion cells in the mouse retina. *J Comp Neurol* 492:66–77
- Völgyi B, Chheda S, Bloomfield SA (2009) Tracer coupling patterns of the ganglion cell subtypes in the mouse retina. *J Comp Neurol* 512:664–687. doi:10.1002/cne.21912
- Völgyi B, Kovács-Öller T, Atlasz T, Wilhelm M, Gábel R (2013a) Gap junctional coupling in the vertebrate retina: variations on one theme? *Prog Retin Eye Res* 34:1–18. doi:10.1016/j.preteyeres.2012.12.002
- Völgyi B, Pan F, Paul DL, Wang JT, Huberman AD, Bloomfield SA (2013b) Gap junctions are essential for generating the correlated spike activity of neighboring retinal ganglion cells. *PLoS ONE* 8:e69426. doi:10.1371/journal.pone.0069426
- Wässle H, Grünert U, Martin PR, Boycott BB (1994) Immunocytochemical characterization and spatial distribution of midget bipolar cells in the macaque monkey retina. *Vision Res* 34:561–579
- Watanabe A (1958) The interaction of electrical activity among neurons of lobster cardiac ganglion. *Jpn J Physiol* 8:305–318
- Xiao M, Hendrickson A (2000) Spatial and temporal expression of short, long/medium, or both opsins in human fetal cones. *J Comp Neurol* 425:545–559